

CED-3 caspase acts with miRNAs to regulate non-apoptotic gene expression dynamics for robust development in *C. elegans*

Authors and Affiliations

Benjamin P. Weaver^{1†}, Rebecca Zabinsky^{1†}, Yi M. Weaver^{1,2}, Eui Seung Lee¹, Ding Xue¹, and Min Han^{1,2}

¹Department of Molecular, Cellular, and Developmental Biology, University of Colorado Boulder.

²Howard Hughes Medical Institute.

†These authors contributed equally to this study.

*Contact: benjaminpweaver@gmail.com

Competing interests: The authors of this study would like to declare no competing interests.

Abstract

Genetic redundancy and pleiotropism have limited the discovery of functions associated with miRNAs and other regulatory mechanisms. To overcome this, we performed an enhancer screen for developmental defects caused by compromising both global miRISC function and individual genes in *C. elegans*. Among 126 interactors with miRNAs, we surprisingly found the CED-3 caspase that has only been well studied for its role in promoting apoptosis, mostly through protein activation. We provide evidence for a non-apoptotic function of CED-3 caspase that regulates multiple developmental events through proteolytic inactivation. Specifically, LIN-14, LIN-28 and DISL-2 proteins are known miRNA targets, key regulators of developmental timing, and/or stem cell pluripotency factors involved in miRNA processing. We show CED-3 cleaves these proteins *in vitro*. We also show CED-3 down-regulates LIN-28 *in vivo*, possibly rendering it more susceptible to proteasomal degradation. This mechanism may critically contribute to the robustness of gene expression dynamics governing proper developmental control.

Introduction

The robustness of animal development is ensured by multiple regulatory mechanisms with overlapping roles acting on specific cellular processes, often manifested as genetic redundancy (Fay et al., 2002; Felix and Wagner, 2008; Kitano, 2004; Hammell et al., 2009). miRNAs mostly exert repression of gene expression by blocking target mRNA translation and/or through mRNA decay as part of the miRNA-induced-silencing

complex (miRISC) which includes GW182 and argonaute proteins (Ding and Han, 2007; Fabian and Sonenberg, 2012). miRNA-mediated gene silencing is a critical regulatory mechanism that ensures dynamic changes in gene expression during animal development or other physiological processes (Bartel and Chen, 2004; Ambros, 2004). However, specific physiological roles of individual miRNAs are often executed through the combinatory effects of multi-miRNA, multi-target mRNA networks (Brenner et al., 2010; Karp et al., 2011; Kudlow et al., 2012; Miska et al., 2007; Parry et al., 2007; Than et al., 2013; varez-Saavedra and Horvitz, 2010). Moreover, these miRNA-mRNA interaction networks may act in concert, and often semi-redundantly, with other regulatory mechanisms to limit the expression of many genes involved in animal development or other physiological functions (Figure1A). Therefore, tackling genetic redundancy would be critical to uncover many specific functions associated with miRNAs and other gene expression regulatory mechanisms.

We have carried out a genome-wide enhancer screen for genes that when knocked down would generate a strong developmental defect when general miRISC function is compromised. Among a large number of interactors identified from the screen is the *ced-3* gene that encodes a caspase, well-characterized as a key component of the apoptotic pathway (Conradt and Xue, 2005). While *ced-3* is absolutely required for the apoptotic process, null mutations of the gene are not associated with obvious developmental defects (Hengartner, 1997). However, two recent studies have reported different non-apoptotic roles of the *ced-3* pathway, namely in stress-related neuronal function (Pinan-Lucarre et al., 2012) and aging (Yee et al., 2014). Because no specific downstream targets of CED-3 were found in these studies, the mechanistic detail of such non-apoptotic functions of CED-3 remains unclear. Moreover, whether the CED-3 system is widely utilized to regulate animal development and other functions is a question of high significance.

Results

A genome-wide enhancer screen to identify factors that act with miRISCs to ensure robust development

To uncover specific physiological functions of miRNAs and other regulatory mechanisms acting with miRNAs during development, we performed a genetic enhancer screen for developmental defects that manifested only when miRISC function and another regulatory mechanism were both compromised (Figure 1A). We chose to use loss-of-function (*lf*) mutations of the *ain-1* and *ain-2* genes (GW182 orthologs) that each alone significantly compromises but does not eliminate global miRISC function (Ding et al., 2005; Zhang et al., 2007; Zhang et al., 2009). While the *ain-1(lf)* mutant has a mild heterochronic phenotype and the *ain-2(lf)* mutant is superficially wild-type, loss of both genes results in severe pleiotropic defects including alteration in temporal cell fate patterning. Therefore, an enhancer screen using the *ain-1(lf)* or *ain-2(lf)* mutant can potentially detect functions associated with most miRNAs.

Using the entire *C. elegans* ORFeome RNAi feeding library (Rual et al., 2004), we performed a double-blind screen that identified 126 genetic interactors (Figure 1A-D, Figure 1—figure supplement 1 and supplemental Tables 1,2), of which only 8 have been reported to interact with miRNA regulatory pathways (Parry et al., 2007). Many interactions were confirmed by testing candidate mutants for phenotypes when treated with *ain-1* and *ain-2* RNAi (supplemental Table 3). Nearly two-thirds of the 126 genetic interactors were found to interact with both *ain-1* and *ain-2* genes (Figure 1B). Gene ontology analysis revealed that these genes belong to a broad range of functional groups (Figure 1C). Over-representation of genes associated with protein stability is consistent with the hypothesis that miRNAs act in concert with other repressive mechanisms to limit gene expression (Figure 1A,C). We found that *ain-1(lf)* displayed more pronounced pleiotropism with its interactors than *ain-2(lf)* (Figure 1D) and that the two GW182 homologs have distinct frequencies of phenotypes with their interactors (Figure 1—figure supplement 1B), arguing against general sickness being the cause for the enhancement (further elaborated in Figure 2—figure supplement 1). The pleiotropic nature of *ain-1* interactions is consistent with the diverse physiological functions associated with AIN-1 or possibly its expression patterns or levels.

Cooperation between the CED-3 pathway and miRISC on multiple aspects of development

We were most surprised to identify the *C. elegans* cell-killing caspase, *ced-3*, as an interactor of the miRISC GW182 homolog, *ain-1*. Using multiple alleles of each gene, we found that *ced-3(lf);ain-1(lf)* double mutants have pleiotropic developmental phenotypes including delays in larval growth rate, smaller brood size, abnormal adult body morphology, egg-laying defect (accumulation of eggs inside the animal), sluggish movement, embryonic lethality, and laid oocytes (failure to fertilize) (Figure 2A-D and Figure 2—figure supplement 2A,B). The penetrance of abnormal phenotypes increased as the adults continued to age (Figure 2—figure supplement 2C) and was therefore best quantified in a synchronized population. Combining mutations of miRISC components such as *ain-1(GW182)(lf)* or *alg-1(argonaute)(lf)* with the cell death pathway factors *ced-3(caspase)(lf)* or its upstream activator, *ced-4(apaf-like)(lf)*, results in abnormal adults (Figure 2E) but *ced-3(lf);ain-2(lf)* animals did not show a significant defect (Figure 2—figure supplement 2D). To test the involvement of other core cell death pathway factors, we also examined the interaction of *ain-1* with *egl-1* that has been shown to act upstream of the CED-3 caspase to promote apoptosis (Figure 2—figure supplement 3A) and *egl-1(lf)* is known to cause a strong cell death defect (Conradt and Xue, 2005). We found that, like *ced-3(lf)* and *ced-4(lf)*, *egl-1(RNAi)* also significantly enhanced the developmental defects of *ain-1(lf)* (Figure 2—figure supplement 3B).

To better characterize these defects, we tested the interaction in specific tissues. Expressing either *ain-1* or *ain-2* in the intestine or hypodermis alone partially rescued the defects of the *ced-3(lf);ain-1(lf)* double mutant (Figure 2F). These findings suggest that these two tissues are the major sites for miRNA functions in this interaction and likely also CED-3 function given that *ced-3* acts cell autonomously (Yuan and Horvitz, 1990). Expressing *ced-3* with strong tissue-specific promoters has been shown to kill those tissues, even in cells that do not normally die, due to the resulting high level of CED-3 accumulation (Shaham and Horvitz, 1996; Hengartner, 1997) thus preventing the reciprocal rescue experiments.

Non-apoptotic functions of *ced-3* caspase in development

The *ced-3* caspase has been well-characterized for its role in apoptosis but not demonstrated to have a broad, non-apoptotic function in development (Yuan et al., 1993; Xue et al., 1996; Peden et al., 2008; Conradt

and Xue, 2005). The fact that strong *ced-3(lf)* alleles cause robust defects in programmed cell death but not the developmental defects described above suggests that the functions of *ced-3* with miRISCs uncovered in our screen are non-apoptotic. To further address this question, we first used an assay previously shown to effectively identify apoptotic functions of genes, such as *mcd-1* encoding a zinc-finger containing protein, for which mutations caused subtle apoptotic defects alone, but significantly enhanced the cell death defect of a *ced-3* reduction-of-function allele (*ced-3(rf)*) (Reddien et al., 2007) (Figure 3A). We found that, in contrast to the positive control, *mcd-1(lf)*, the *ain-1(lf)* mutation did not enhance the apoptotic defect of *ced-3(rf)* animals as assayed by observing the perdurance of *lin-11::GFP* positive undead P9-11.aap cells (Figure 3A-B). Because *nuc-1* encodes an effector nuclease important for the proper execution of apoptosis (Wu et al., 2000), we then tested if the *ain-1(lf)* mutation was able to enhance any subtle *nuc-1(lf)* phenotype and found no significant defect beyond the phenotypes of the single mutants (Figure 3C). Finally, *ain-1(RNAi)* did not affect the number of apoptotic cell corpses accumulating in the heads of *ced-1(lf)* first stage larvae (Figure 3D), which are defective in cell corpse engulfment allowing for visualization of dead cell corpses. Therefore, the *ain-1* and *ced-3* interaction described above is non-apoptotic.

Function of *ced-3* caspase in temporal cell fate patterning

Further analysis indicated that the *ced-3(lf)* and *ced-4(lf)* single mutants have mild reduction in their rates of post-embryonic growth similar to the *ain-1(lf)* and *alg-1(lf)* mutants (Figure 4A-C and also Figure 4—figure supplement 1 for more *ced-3(lf)* data). Additionally, the *ced-3(lf);ain-1(lf)* and *ced-3(lf);alg-1(lf)* double mutants, but not *ced-3(lf);ain-2(lf)*, have significantly slower growth rates beyond either single mutant (Figure 4A-C and Figure 4—figure supplement 1), suggesting cooperativity in regulating the related developmental programs.

To interrogate the genetic interaction further, we screened all of the available *C. elegans* miRNA deletion strains in the blind (Figure 5A, strains listed in supplemental Table 4) for synthetic interactions with *ced-3* by depleting *ced-3* in each miRNA mutant background by RNA interference. After finding pronounced RNAi effects associated with several miRNA deletions, we then generated double or triple mutants containing

ced-3(lf) and the miRNA mutations, and observed phenotypes similar to those seen in *ced-3(lf);ain-1(lf)* (Figure 5B, and refer to Figure 2A-E). Specifically, mutations in the *let-7*-family members, *mir-48* and *mir-84*, had the strongest effect with a fully penetrant egg-laying defect observed in the *ced-3(lf);mir-48(lf);mir-84(lf)* triple mutant (Figure 5B). Interestingly, the *ced-3(lf);mir-1(lf);mir-84(lf)* triple mutant displayed some developmental defects not seen in the *mir-1(lf);mir-84(lf)*, *ced-3(lf);mir-1(lf)*, or the *ced-3(lf);mir-84(lf)* double mutants (Figure 5B). Since *ced-3(lf)* had the strongest developmental defects with the *let-7*-family members, and since both *lin-14* and *lin-28* mRNAs are well-known targets of the *let-7*-family of miRNAs, we thus tested the possibility that *ced-3(lf)* may enhance specific temporal cell fate patterning defects of these miRNA mutants by examining their adult alae. Normal adult-specific alae are generated by seam cells and defects in adult alae formation were commonly used as a sensitive assay for defects in temporal cell fate patterning (Ambros and Horvitz, 1984). We found that *ced-3(lf)* significantly enhanced adult alae defects (Figure 5C,D). This effect was observed for both the *miR-48(lf),miR-84(lf);ced-3(lf)* triple mutant and the *ced-3(lf);ain-1(lf)* double mutant, but not the *ced-3(lf);mir-1(lf);mir-84(lf)* triple mutant (Figure 5D). These findings suggested the hypothesis that the expression of some developmental timing regulators is co-regulated by miRISCs and *ced-3*.

Negative regulation of the pluripotency factors *lin-14*, *lin-28*, and *disl-2* by *ced-3*

To better analyze the mechanism underlying this non-apoptotic temporal cell fate patterning function of *ced-3*, we tested its effect on seam cell development. The division and differentiation pattern of the stem cell-like seam cells are regulated by a well-described genetic pathway that includes several miRNAs and the LIN-28 pluripotency factor that blocks the maturation of pre-*let-7* miRNA (Viswanathan and Daley, 2010). During each larval stage, lateral seam cells (V1-V4 and V6) divide in an asymmetric, stem-cell like manner with additional stem cells only produced in the L2 stage by an additional symmetric division pattern that duplicates V1-V4 and V6 seam cell numbers (Ambros and Horvitz, 1984; Sulston and Horvitz, 1977). Wild-type animals consistently have 16 seam cells on both the left and right sides by adulthood (Joshi et al., 2010). The dynamic changes in the expression levels of several conserved pluripotency factors is critical for proper temporal cell fate patterning. LIN-14 is highly expressed during L1 to promote L1-specific developmental programs, whereas

161 LIN-28 is highly expressed from late embryonic to L2 stages and acts to promote the L2-specific programs
162 including the only normal symmetric division of V1-V4 and V6 seam cells (Ambros and Horvitz, 1984; Ambros,
163 1989; Ruvkun and Giusto, 1989; Moss et al., 1997; Rougvie and Moss, 2013) (diagrammed in Figure 6—figure
164 supplement 2A). Expression of LIN-14 and LIN-28 rapidly diminishes after L1 and L2, respectively, which is
165 necessary for animals to progress to the next stage (Figure 6—figure supplement 2A). Loss-of-function (*lf*)
166 mutations in *lin-14* and *lin-28* result in animals skipping the L1- and L2-specific programs, respectively
167 (precocious phenotype) (Figure 6—figure supplement 2A). In contrast, hyperactive (gain-of-function, *gf*)
168 mutations leading to prolonged expression of each gene cause the animals to reiterate the corresponding
169 stage (retarded phenotype) (Figure 6—figure supplement 2A). Because of the additional symmetric cell
170 division of V1-V4 and V6 seam cells in L2, skipping or reiterating the L2 stage in *lin-28(lf)* or *lin-28(gf)*
171 mutations lead to a decrease or increase of total seam cell number, respectively (Ambros and Horvitz, 1984;
172 Moss et al., 1997) and diagrammed in Figure 6—figure supplement 2A.. Mammalian DIS3L2 was recently
173 annotated as the ribonuclease that degrades the uridylated pre-*let-7* miRNA following binding by LIN-28 and
174 3'-oligo-uridylation by a polyU polymerase (Chang et al., 2013). We identified the likely *C. elegans* ortholog of
175 Dis3l2 and named it *disl-2* (Figure 6—figure supplement 1). The effects for *disl-2* on seam cell development
176 have not been determined.

177 As previously published (Ding et al., 2005; Zhang et al., 2007), we also found that the *ain-1(lf)* mutant
178 alone has a mild increase in the number of seam cells by late larval development (Figure 6A,B and Figure 6-
179 figure supplement 2) consistent with the well-established role of miRNAs in regulation of temporal cell fate
180 patterning; whereas the *ced-3(lf)* mutant alone rarely shows altered seam cell numbers (Figure 6A,B and
181 Figure 6—figure supplement 2). Strikingly, the *ced-3(lf);ain-1(lf)* double mutants have both a markedly
182 increased number of seam cells and an increased range of seam cell number by late larval development
183 (Figure 6A,B) with a mean value (\pm SD) of 25.9 (\pm 5.5) per side. Notably, the *ced-3(lf);ain-1(lf)* double mutants
184 hatch with the correct number of seam cells but they continue to increase inappropriately throughout later
185 larval development (Figure 6—figure supplement 2A,B). The production of supernumerary seam cells indicates
186 a previously unknown role for *ced-3* in cooperating with miRISC-regulated seam cell differentiation and
187 temporal cell fate patterning (Figure 6A,B and Figure 6—figure supplement 2B)..

We found that the increased number of seam cells in the *ced-3(lf);ain-1(lf)* double mutants was partially suppressed by down-regulating *lin-14*, *lin-28*, or *disl-2(Disl2)* through RNAi treatment beginning at L2 (Figure 6C), suggesting that an abnormally high level of any of the three proteins could be a significant contributor to the phenotype. A *lin-14(lf)* or *lin-28(lf)* mutation would not be effective for such a suppression test because of the strong defects associated with them at the early larval stage (Moss and Tang, 2003). LIN-66 was previously shown to act in parallel to miRNAs to repress LIN-28 expression (Morita and Han, 2006). Consistent with a *ced-3* function in *lin-28*-mediated temporal cell fate patterning regulation, we also observed that *ced-3(lf)* enhanced the heterochronic defect of *lin-66* reduction (Figure 6—figure supplement 3). We further found that down-regulation of *lin-14*, *lin-28*, or *disl-2(Disl2)* by RNAi beginning at L2 could significantly suppress the defects in the *ced-3(lf);ain-1(lf)* double mutants (Figure 6D). These findings suggest that *ced-3* cooperates with miRNAs to regulate the *lin-14-lin-28-disl-2(Disl2)* axis during development.

Cleavage of LIN-14, LIN-28, and DISL-2 *in vitro* by CED-3

The above genetic data suggest that *ced-3* normally represses *lin-28*, *disl-2* and/or *lin-14* in development. As a caspase, we thought that CED-3 may directly repress the expression of these genes through proteolytic cleavage, which is consistent with our observation that LIN-14, LIN-28, and DISL-2 contain multiple consensus CED-3 cleavage sites that consist of a tetra-peptide sequence usually ending in an aspartic acid residue (Xue et al., 1996). To test this hypothesis, we performed an *in vitro* CED-3 cleavage assay as previously described (Xue et al., 1996). We found that the DIS3L2 ribonuclease homolog, DISL-2, was robustly cleaved by the CED-3 caspase while LIN-14 and LIN-28 were partially cleaved (Figure 7A). The multiple cleavage products generated by CED-3 cleavage of DISL-2 (Figure 7A,B) suggest a clear role for CED-3-mediated inactivation of this target protein. We further tested the specificity of the partial LIN-28 cleavage by CED-3 and found that it was completely blocked by addition of the caspase-specific-inhibitor zDEVD-fmk (Figure 7C). We then determined the proteolytic cleavage site for LIN-28 by mutagenesis and identified the CED-3-specific recognition sequence (Figure 7D and Figure 7—figure supplement 1). Numerous possible cleavage sites were found for LIN-14 and DISL-2 but were not pursued further (Figure 7—figure supplement

2). The identified sequence DVVD fits the canonical CED-3 recognition motif (DxxD) (Xue et al., 1996) and mutating the second aspartic acid residue to an alanine (D31A in Figure 7D) entirely eliminated CED-3 cleavage. CED-3 proteolysis of LIN-28A generates an N-terminal asparagine in the remaining protein (Figure 7E). Asparagine is known to function generally as a destabilizing residue at the N-terminus of eukaryotic proteins resulting in proteasomal degradation in a phenomenon termed the N-end rule (Sriram et al., 2011).

CED-3 impact on LIN-28 turnover *in vivo*

To examine CED-3-mediated turnover of the LIN-28 protein *in vivo*, we generated a polyclonal antibody against a C-terminal peptide in LIN-28 that recognizes both LIN-28 isoforms reported previously (Seggerson et al., 2002) (Figure 8—figure supplement 1A,B). We found that the dynamic decrease in LIN-28 abundance during L2-L4 stages was similarly delayed by two different *ced-3(lf)* mutations (Figure 8A and quantitation shown in Figure 8—figure supplement 1C). At late L4 (48 hr in Figure 8A), LIN-28 was almost completely absent in both wild type and *ced-3(lf)* mutants, indicating the role of general, non-CED-3-mediated, proteolysis during late larval stages. Interestingly, the 22 kDa cleavage product observed in the *in vitro* assay (Figure 7D,E) was not observable *in vivo* (Figure 8A), consistent with the idea that the cleavage product with an asparagine at its N-terminus was possibly degraded by an additional proteolytic process. It is possible that the delayed down-regulation of LIN-28 seen in Figure 8A is the consequence of the slower post-embryonic growth rate observed for *ced-3(lf)* mutants (Figure 4). To address this question, we first used a LIN-28::GFP transgenic strain previously shown to have functional LIN-28 activity (Moss et al., 1997) to monitor stage-matched L3 larvae with or without a *ced-3(lf)* mutation by DIC microscopy. We observed that the *ced-3(lf)* mutation delayed the proper down-regulation of the LIN-28::GFP reporter at L3 in the hypodermis (Figure 8B-D and Figure 8—figure supplement 2A-C). We also found that down-regulation of LIN-28::GFP expression was delayed in neuronal cells in the head (Figure 8—figure supplement 2D,E). These findings support the hypothesis for the delayed down-regulation of LIN-28 by *ced-3(lf)*. The difference in magnitude between the Western blot results and the number of fluorescent cells seen by DIC microscopy may suggest that the

observed fluorescence levels do not linearly reflect the protein levels and that the two methods may have different dynamic ranges..

We then further addressed the question by testing the physiological impact of the *lin-28(D31A)* mutation. Specifically, we made the point mutation in the previously published *lin-28(+):gfp* fusion protein (Moss et al., 1997). To ensure that the LIN-28(D31A) mutation did not disrupt the global function of the protein, we tested its ability to rescue the highly penetrant protruding vulva (Pvl) phenotype in *lin-28(n719,lf)* animals and found that it was able to rescue the Pvl phenotype (Figure 9—figure supplement 1). Following integration and outcrossing, we found the copy number of the *lin-28(D31A):gfp* transgene to be slightly lower than that of the non-mutated *lin-28(+):gfp* transgene (Figure 9—figure supplement 2). We then examined the developmental profile and found that the *lin-28(D31A):gfp* transgene alone caused a delay in larval development similar to that caused by the combination of the *lin-28(+):gfp* transgene with *ced-3(lf)* (Figure 9A). Western blot analysis showed that the *lin-28(D31A):gfp* integration had less basal expression than the non-mutated *lin-28(+):gfp* integration, consistent with the lower copy number estimate. We observed a quantifiable difference in the down-regulation of the *lin-28(D31A):gfp* transgene compared to the *lin-28(+):gfp* transgene (Figure 9B,C). This finding provides evidence that a failure in CED-3 cleavage of LIN-28 leads to slower degradation of LIN-28 and is one of the causes of slower development, since the D31A point mutation alone resulted in both a slower growth rate (Figure 9A) and delayed LIN-28 down-regulation (Figure 9B,C). Additionally, in this Western blot (Figure 9B-C), down-regulation of the wild-type LIN-28 transgene in *ced-3(lf)* worms seems to be delayed more than LIN-28(D31A) in wild type worms. Such a difference could be due to roles of CED-3 on other targets such as LIN-14 and DISL-2, which is also expected to contribute to the larval developmental defect in *ced-3(lf)* (Figure 9A).

Examination of adult-specific alae is a sensitive physiological readout that should overcome any limitations of monitoring delays in the down-regulation of LIN-28 expression levels since scoring adult alae ensures stage-matching and accounts for any perdurance. To further test the functional outcome of both the LIN-28(D31A) transgene and the LIN-28(+) transgene combined with *ced-3(lf)*, we examined the adult-specific alae and found significant defects including low quality and gapped alae (Figure 9D and Figure 9—figure

supplement 3). This is consistent with the data described above that *ced-3(lf)* enhances adult-specific alae defect of let-7-family miRNA mutants and *ain-1(lf)* (Figure 5C-D). We should note that the original report of the LIN-28(+) transgene indicated that some of the adults were observed to have gapped alae (Moss et al., 1997). Though we did observe rough and very thin sections of alae for this strain (scored as low quality alae), we did not observe any gapped adult alae. This subtle difference is likely explained by a different threshold since we scored alae using a sensitive camera (See Methods). Nonetheless, the relative enhancement of *ced-3(lf)* with this transgene is quite obvious and similar to that of the caspase-cleavage resistant LIN-28(D31A) point mutant transgene (Figure 9D). Altogether, our data support a causal role for CED-3 cleavage of LIN-28 in the regulation of temporal cell fate patterning. CED-3 appears to facilitate the stereotypical transition of LIN-28 to enhance the robustness of the L2 to L3 developmental transition.

Consistent with LIN-14 being modestly cleaved by CED-3 *in vitro* (Figure 7A), we found that the LIN-14::GFP level was modestly increased in *ced-3(lf)* mutants *in vivo* at the L1 stage (Figure 9—figure supplement 4). This result may not be explained by slower growth rate since these animals were obtained as synchronous L1s without food. Our attempts to monitor DISL-2 protein levels including developing an antibody to endogenous DISL-2 were impeded by technical difficulties. Moreover, N- and C-terminal GFP fusions to DISL-2 had exceedingly low levels of expression beyond detection by common methods suggesting that DISL-2 protein levels are kept exquisitely low for physiological significance.

Therefore, our *in vitro* and *in vivo* data show that developmental timing regulators are proteolytic targets of the CED-3 caspase, likely resulting in their inactivation. This role of CED-3 cleavage is in contrast to known apoptotic functions of CED-3 caspase activity in two major aspects: CED-3 inactivates its targets rather than activates them as in its apoptotic function (Conradt and Xue, 2005); and it acts with other regulatory systems, including miRNAs and possibly the N-end rule proteasomal system, to maintain robust developmental functions.

Discussion

Role of non-apoptotic CED-3 activity in enhancing the robustness of dynamic changes in gene expression for development

We report the discovery of a new gene expression regulatory mechanism whereby a non-apoptotic activity of the CED-3 caspase functions to inactivate and repress the expression of key developmental regulators, significantly contributing to the robustness of gene expression dynamics and animal development (Figure 10A). Consistent with this, a previous report showed that CED-3 is capable of cleaving more than twenty-two *C. elegans* proteins in an *in vitro* proteomics survey (Taylor et al., 2007) and two recent genetics-based findings showed that *ced-3* may play important roles in neural regeneration (Pinan-Lucarre et al., 2012) and aging (Yee et al., 2014). Second, the described CED-3 function in repressing gene expression is likely in contrast to the role of CED-3 in promoting apoptosis through activation of protein targets by cleavage at specific sites (Nakagawa et al., 2010; Chen et al., 2013). Here, the CED-3 cleavage alone may already destroy the target protein activity. Additionally, the cleavage products may be further degraded by other degradation systems notably via N-terminal destabilizing residues which may make the target more susceptible to additional degradation mechanisms, such as proteasomal degradation (Sriram et al., 2011) (Figure 10B). We hypothesize that this function operates continually during development to facilitate rapid turnover of these regulatory proteins at the post-translational level and in cooperation with other regulatory mechanisms (Figure 10—figure supplement 1). We should note that it is curious that only the LIN-28A isoform was found to be cleaved by CED-3 *in vitro* yet expression of both LIN-28A and LIN-28B isoforms was altered by *ced-3(lf)* *in vivo*. This may imply that *ced-3* has potential indirect effects on other factors within the heterochronic pathway that could alter LIN-28 isoform expression but further experiments are required to satisfactorily explain this.

We find that the altered LIN-28 expression levels in a *ced-3(lf)* background, or with the caspase-cleavage resistant mutant [LIN-28(D31A)] in a *ced-3(wt)* background, are subtle compared to previous findings regarding a *lin-28(gf)* transgene with deleted *lin-4* and *let-7* miRNA-binding sites in the 3' UTR (Moss et al., 1997). Consistent with this subtlety, *ced-3(lf)* alone displays essentially no defect in seam cell numbers (Figure 6). The physiological effect of this subtle regulation is clearly seen in seam cell temporal patterning when miRNA function is compromised in the *ain-1(lf)* mutant background. This prominent enhancement indicates

that *ced-3* has an important role in supporting the robustness of the larval transitions. Based on the pleiotropic phenotypes associated with *ced-3(lf); ain-1(lf)*, such roles may potentially extend to a broad range of cellular processes.

Cooperative gene regulation revealed by our genome-scale screen

Previous studies using model organisms, including our own, have indicated that genetic redundancy by structurally unrelated genes is commonly associated with genes with regulatory functions (Suzuki and Han, 2006; Fay et al., 2002; Costanzo et al., 2011; Ferguson et al., 1987). Asking the same question for the global miRISC function, our screen, by identifying 118 previously unknown miRISC interactors, thus identified new roles for miRISC in normal developmental processes that are otherwise masked by redundancy and/or pleiotropism, as well as identifying other regulatory mechanisms that collaborate with miRNAs. Examples we found for the latter in this study include genes encoding the POU-homeodomain protein (*ceh-18*, Figure 2—figure supplement 1), the histone acetyltransferase (*pcaf-1*), the ras-related GTPase homolog (*ral-1*), the homeodomain transcription factor (*unc-39*), and the cell-killing *ced-3* caspase (the majority of this study) (and others listed in supplemental Table 2). However, the interactions identified in this study most likely reflect only a small portion of miRNA functions because screening for obvious developmental defects under well-fed conditions only permitted us to identify limited physiological functions. Applying various assays, including behavioural assays or animals under various growth or stress conditions, is expected to identify many more miRNA functions. Furthermore, although feeding RNAi has important advantages for such a screen, it is not effective for many genes especially for genes functioning in certain tissues such as neurons. Therefore, genetic screens or analyses under sensitized backgrounds will continue to play a major role in identifying miRNA functions.

Materials and methods

***C. elegans* strains**

See supplemental Table 4 for the list of all strains used in this study.

Rationale of phenotypes scored in this screen

In this screen, we wanted to identify genetic pathways that may redundantly cooperate with the miRISC in development. Since the loss of most miRISC function resulted in highly pleiotropic phenotypes (Zhang et al., 2009), we chose to score multiple obvious phenotypes (defined in supplemental Table 1).

Genome-wide, double blind RNAi screen

The ORFeome RNAi feeding library (Rual et al., 2004) was screened using a 96-well liquid culture format in the double blind. Here, double blind means that no identities for interactors were revealed to anyone setting up the plates, anyone phenotyping the plates, nor anyone processing the scored data until all candidate interactors were confirmed in a secondary screen performed in quadruplicate (see below). Similar to a previously reported method (Lehner et al., 2006), a two day set up for each screening session was employed (Figure 1—figure supplement 1A).

For each scoring session, *rff-3(pk1426,lf)*, *ain-1(ku322,lf);rff-3(pk1426,lf)*, and *ain-2(tm2432,lf);rff-3(pk1426,lf)* were each fed with mock, *ain-1*, and *ain-2* RNAi cultures in parallel which served as the experimental controls. These controls were set up in 4 sets of triplicate (n=12 total for each). We identified potential interactors whenever *ain-1(ku322);rff-3(pk1426)* or *ain-2(tm2432);rff-3(pk1426)* showed a significant defect (Figure 1—figure supplement 1A). All candidates were then retested in quadruplicate liquid format. Any gene showing effect in 3 or more replicates was considered a *bona fide* interactor by RNAi and their identities were then revealed and confirmed by sequence analysis. Multiple interactors were confirmed by testing the corresponding mutant strains when treated with *ain-1* or *ain-2* RNAi (supplemental Table 3).

Statistical analyses

Before any statistical analyses were made, all relevant data sets were first tested for normality using the D'Agostino-Pearson omnibus test. This test also informed us for sufficient sample sizes. We analyzed our results in the following ways: 1) the Mann-Whitney test was used for pair-wise comparisons, 2) Chi-square analysis was used to compare distributions of categorical data, and 3) Fisher's Exact test was used to analyze

cases where two categories were most important between two strains (e.g. the frequency of normal animals to the pooled frequency of all abnormal animals in each of the tissue-specific rescues or in the RNAi suppression test). Use of Fisher's Exact test in such cases prevented outcomes where Chi-square analysis of the same data may identify a rescue as significant only because the abnormal phenotypic categories had changed in distribution relative to the unrescued mutant, but where the fraction of normal animals was not improved. P values and statistical tests were reported throughout the study. Statistics source data have been provided.

RNAi treatment by feeding on solid agar

Similar to the liquid culture format, positive and negative controls were run in parallel to ensure effectiveness of the culturing conditions. RNAi cultures and plates were prepared as previously described (Fraser et al., 2000; Timmons et al., 2001) with 100 µg/ml ampicillin. Depending on the experiment, strains were added to RNAi plates in one of the following ways: 1) bleached strains were synchronised in M9 for 36 hours at 20°C, counted, then added to plates or 2) eggs, L2 stage animals, or L4 stage animals were carefully added to lawns.

Counting percent of eggs hatched after RNAi treatment

Gravid young adult *ain-1(lf)* hermaphrodites fed either mock or *ced-3* RNAi since hatching were transferred to a new RNAi plate and allowed to lay eggs for 4-5 hours. The young adults were removed and the eggs laid were counted. After 40 hours at 20°C, unhatched eggs and larvae were scored. 64 hours after removing young adults, very few additional larvae were observed for *ain-1(lf)* animals treated with *ced-3* RNAi. Data are from eight independent trials.

Assay for the rates of post-embryonic development

Synchronous L1 stage animals were added to normal food (OP50 bacteria) (150-200 worms per trial) and incubated at 20°C. Animals were scored for developmental stages every 24 hours thereafter. Data are from three to five independent trials.

Tissue-specific rescue of *ain-1(lf)*

The *ain-1(lf)* defects were rescued using a fragment of genomic DNA containing *ain-1* sequence and native promoter (Ding et al., 2005), an *ain-1* sequence driven by a *dpy-5* (hypodermal-specific (Thacker et al., 2006)) or a *ges-1* (gut-specific (Egan et al., 1995)) promoter, and genome-integrated constructs with tissue-specific promoters driving *ain-2* expression which has previously been shown by our lab to rescue *ain-1(lf)* in those tissues (Zhang et al., 2011; Than et al., 2013; Kudlow et al., 2012). Data are from four to ten independent trials.

Enhancer screen for *miRNA* deletion mutants with *ced-3* RNAi

In the blind, all available miRNA deletion mutants were tested for enhancer phenotypes with *ced-3* using the RNAi feeding method on solid agar. The *let-7(lf)* mutant was excluded since it is very sick. One person picked ten eggs or two L4 stage animals onto mock or *ced-3* RNAi in replicates according to a key that was kept confidential. Four to five days later, another person then examined the plates for phenotypes (defined in supplemental Table 1). All mutants showing an RNAi phenotype were revealed for identity and then crossed with *ced-3(lf)* mutants in single or in combination and tested for enhancer phenotypes.

Apoptotic assay and rationale

We employed a published assay to identify subtle apoptotic enhancers using a reporter line: *ced-3(n2427, reduction of function);nls106 [lin-11::GFP + lin-15(+)]* (Reddien et al., 2007). The *ced-3(n717);nls106* strain served as the positive control for complete loss of *ced-3* function, and the *mcd-1(n3376);ced-3(n2427,rf);nls106* strain was the positive control for enhanced ablation of programmed cell death comparable to the strong *ced-3(n717)* loss of function allele for accumulation of P9-11.aap cells, consistent with the previous findings (Reddien et al., 2007). Young adults of all strains were scored in the blind for the number of GFP-positive undead P9-11.aap ventral cord cells. Three independent lines of *ced-3(n2427,rf);ain-1(lf);nls106* were scored in the blind (data for these three lines were combined in Figure 3B).

L1 stage cell-corpse assay

This standard method was done as previously described (Ledwich et al., 2000). The *ced-1(e1735)* mutation was used to enhance visualization of corpses. DIC optics were used to count the head corpses.

3' UTR miRNA seed site prediction

These predictions were all made by TargetScan 6.2 release June 2012 (Jan et al., 2011; Lewis et al., 2005).

Scoring adult-specific alae

Adult alae were scored using DIC optics (Zeiss Axioplan 2) at 630x magnification (Ding et al., 2005; Zhang et al., 2007; Zhang et al., 2009). One side of each non-roller adult was scored (the side facing up). All roller phenotype animals (the three LIN-28::GFP transgenic lines) were scored in the same way such that all alae that could be viewed were assessed for gaps and quality. Each animal was scored as either normal, low quality alae (very thin and rough sections), or gapped alae (discontinuous alae). Animals with both low quality and gapped alae were counted as only gapped alae so that each animal was represented only once. Any thin region of alae that appeared as a gap through the oculars was imaged by the camera (Zeiss AxioCam MRm) and evaluated on a large screen. Only alae observed as truly discontinuous by aid of the camera were scored as gapped. This method was applied equally to all strains throughout the study.

Seam cell counting method

All seam cell lines were counted on a fluorescent microscope with DIC optics (Zeiss Axioplan 2) at 110x and 630x magnification (Zhang et al., 2009) at the L1, L3 or L4 stage. To prevent over-representation of our sample size, we reported only one side of each animal. We randomly chose to report the top or the left side of the animal, depending on the orientation in the microscopy field. We followed this convention for the single mutants as well. Therefore, one dot corresponds to one side of one animal and each animal is plotted only once (Figure 6A-C and Figure 6—figure supplement 2). Data are from five independent trials.

RNAi suppression test

We hypothesized that loss of both *ain-1* and *ced-3* resulted in the upregulation of LIN-14, LIN-28, and DISL-2. These factors are normally expressed at high levels beginning in late embryonic development and down-regulated toward the end of the second larval stage. We therefore decided to begin RNAi treatment of *ced-3(lf);ain-1(lf)* animals at the second larval stage and score for phenotypes 48-54 hours later. Animals were considered normal if they were only mildly-to-moderately egg-laying defective and capable of normal motility. Data are from three to six independent trials.

CED-3 *in vitro* cleavage assay

The LIN-14, LIN-28, and DISL-2 coding sequence templates for *in vitro* synthesis were each generated first by reverse transcription from mixed stage WT (N2) *C. elegans* total RNA and then PCR amplified before subcloning into pTNT vector (Promega). The primer sequences are as follows (restrictions sites indicated in bold-type, start codons underlined in FWD primers): *lin-14* FWD, **attacgcgt**ACCATGGCTATGGATCTGCCTGGAACGTCTTCGAAC; REV, **attggtacc**CTATTGTGGACCTTGAAGAGGAGGAG; *lin-28* FWD, **attacgcgt**ACCATGGCTATGTCGACGGTAGTATCGGAGGGA; REV, **attggtacc**CTCAGTGTCTAGATGATTCTATTCATC; *disl-2* FWD, **attacgcgt**ACCATGGCTATGTCAGCAGTTGAAAGTCCCGTT; REV, **attggtacc**CTACTGAAGAATTGTTGAGCCCGTTTC. Point mutations were generated using Quick Change II kit (Agilent Technologies, www.genomics.agilent.com/). All constructs were sequence-verified. As previously published (Xue et al., 1996), cleavage substrates were freshly synthesised with L-³⁵S-Methionine *in vitro* and used immediately. For caspase inhibitor reactions, zDEVD-fmk caspase-specific inhibitor (ApexBio, www.apexbt.com) or DMSO was added. All cleavage reactions were incubated at 30°C in a thermocycler with heated lid for up to 6 h. Each panel shown in Figure 7 was performed independently with freshly synthesized L-³⁵S-labeled substrates and independent cleavage reactions for each experiment.

LIN-28 antibody and Western blot

Antibody against a LIN-28 C-terminal peptide (RKHRPEQVAAEEAEA) was produced by Spring Valley Laboratories using rabbit as the host and purified using a peptide column. Validation of the specificity of the antibody is shown in Figure 8—figure supplement 1A,B. Synchronous L1 stage animals were added to normal food (OP50 bacteria) and incubated at 20°C then collected at the indicated hours with food. For each time-point, equivalent protein input from wt, *ced-3(n717)*, and *ced-3(n1286)* staged animal lysates were resolved by SDS-PAGE and then detected by Western blot using the anti-LIN-28 antibody. Actin was used as loading control (Anti-Actin antibody, A2066, Sigma-Aldrich).

Scoring LIN-28::GFP positive cells by DIC optics

Similarly sized L3 stage animals were picked on a non-fluorescent dissecting scope to blind the selection of animals. Prior to fluorescent illumination, gonad length was observed and measured to ensure animals were of comparable developmental stage (Ambros and Horvitz, 1984; Moss et al., 1997; Abbott et al., 2005). This method should provide a similar distribution of developmental sub-stages for both backgrounds within the L3 stage. No significant difference in gonad extension was found (Figure 8—figure supplement 2A-C). Gonad length was measured and recorded prior to GFP illumination to ensure no bias. All animals were illuminated for 5 seconds for each picture by DIC optics. Multiple planes through the animal were examined by one person to ensure all GFP positive cells were identified. Another person, who did not take the images, then used Image J to obtain integrated GFP intensity values which were reported relative to the gonad length to account for stage (Figure 8B-D) or counted the number of GFP positive head cells (Figure 8—figure supplement 2D, E). Data for all animals viewed by DIC were kept and reported. Data for the hypodermal and head cell expression assays come from two and three independent experiments, respectively.

Acknowledgments

We thank R. Horvitz, S. Mitani, V. Ambros, and the CGC (funded by NIH Office of Research Infrastructure Programs (P40 OD010440)) for strains; E. Moss for materials; A. Fire for vectors; V. Ambros, W. Wood, R. Yi,

S. Park, M. Kniazeva, M. Cui, and Han lab members for discussions; and A. Sewell for comments. Supported by the postdoctoral fellowship 121631-PF-12-088-01-RMC from the American Cancer Society (BPW), NIH grants 5R01GM047869 (MH), R01GM059083 (DX), and 2T32GM008759-11 (RZ). The authors of this study would like to declare no competing financial interests. The funding agencies had no role in study design, data collection, interpretation of the results, the decision to publish, or preparation of the manuscript.

References

- Abbott,A.L., varez-Saavedra,E., Miska,E.A., Lau,N.C., Bartel,D.P., Horvitz,H.R., and Ambros,V. (2005). The let-7 MicroRNA family members mir-48, mir-84, and mir-241 function together to regulate developmental timing in *Caenorhabditis elegans*. *Dev. Cell* 9, 403-414.
- Ambros,V. (1989). A hierarchy of regulatory genes controls a larva-to-adult developmental switch in *C. elegans*. *Cell* 57, 49-57.
- Ambros,V. (2000). Control of developmental timing in *Caenorhabditis elegans*. *Curr. Opin. Genet. Dev.* 10, 428-433.
- Ambros,V. (2004). The functions of animal microRNAs. *Nature* 431, 350-355.
- Ambros,V. and Horvitz,H.R. (1984). Heterochronic mutants of the nematode *Caenorhabditis elegans*. *Science* 226, 409-416.
- Arasu,P., Wightman,B., and Ruvkun,G. (1991). Temporal regulation of lin-14 by the antagonistic action of two other heterochronic genes, lin-4 and lin-28. *Genes Dev.* 5, 1825-1833.
- Bartel,D.P. and Chen,C.Z. (2004). Micromanagers of gene expression: the potentially widespread influence of metazoan microRNAs. *Nat. Rev. Genet.* 5, 396-400.
- Brenner,J.L., Jasiewicz,K.L., Fahley,A.F., Kemp,B.J., and Abbott,A.L. (2010). Loss of individual microRNAs causes mutant phenotypes in sensitized genetic backgrounds in *C. elegans*. *Curr. Biol.* 20, 1321-1325.
- Chang,H.M., Triboulet,R., Thornton,J.E., and Gregory,R.I. (2013). A role for the Perlman syndrome exonuclease Dis3l2 in the Lin28-let-7 pathway. *Nature* 497, 244-248.
- Chen,Y.Z., Mapes,J., Lee,E.S., Robert Skeen-Gaar,R., and Xue,D. (2013). Caspase-mediated activation of *Caenorhabditis elegans* CED-8 promotes apoptosis and phosphatidylserine externalization. *Nat. Commun.* 4, 2726.
- Conradt,B. and Xue,D. (2005). Programmed cell death. *WormBook*. 1-13.
- Costanzo,M., Baryshnikova,A., Myers,C.L., Andrews,B., and Boone,C. (2011). Charting the genetic interaction map of a cell. *Curr. Opin. Biotechnol.* 22, 66-74.
- Ding,L. and Han,M. (2007). GW182 family proteins are crucial for microRNA-mediated gene silencing. *Trends Cell Biol.* 17, 411-416.
- Ding,L., Spencer,A., Morita,K., and Han,M. (2005). The developmental timing regulator AIN-1 interacts with miRISCs and may target the argonaute protein ALG-1 to cytoplasmic P bodies in *C. elegans*. *Mol. Cell* 19, 437-447.
- Egan,C.R., Chung,M.A., Allen,F.L., Heschl,M.F., Van Buskirk,C.L., and McGhee,J.D. (1995). A gut-to-pharynx/tail switch in embryonic expression of the *Caenorhabditis elegans* ges-1 gene centers on two GATA sequences. *Dev. Biol.* 170, 397-419.
- Fabian,M.R. and Sonenberg,N. (2012). The mechanics of miRNA-mediated gene silencing: a look under the hood of miRISC. *Nat. Struct. Mol. Biol.* 19, 586-593.
- Fay,D.S., Keenan,S., and Han,M. (2002). fzf-1 and lin-35/Rb function redundantly to control cell proliferation in *C. elegans* as revealed by a nonbiased synthetic screen. *Genes Dev.* 16, 503-517.

544 Felix,M.A. and Wagner,A. (2008). Robustness and evolution: concepts, insights and challenges from a
545 developmental model system. *Heredity* (Edinb.) 100, 132-140.

546 Ferguson,E.L., Sternberg,P.W., and Horvitz,H.R. (1987). A genetic pathway for the specification of the vulval
547 cell lineages of *Caenorhabditis elegans*. *Nature* 326, 259-267.

548 Fraser,A.G., Kamath,R.S., Zipperlen,P., Martinez-Campos,M., Sohrmann,M., and Ahringer,J. (2000).
549 Functional genomic analysis of *C. elegans* chromosome I by systematic RNA interference. *Nature* 408, 325-
550 330.

551 Hammell,C.M., Karp,X., and Ambros,V. (2009). A feedback circuit involving let-7-family miRNAs and DAF-12
552 integrates environmental signals and developmental timing in *Caenorhabditis elegans*. *Proc. Natl. Acad.*
553 *Sci. U. S. A* 106, 18668-18673.

554 Hengartner,M.O. (1997). Cell Death.

555 Hochbaum,D., Zhang,Y., Stuckenholtz,C., Labhart,P., Alexiadis,V., Martin,R., Knolker,H.J., and Fisher,A.L.
556 (2011). DAF-12 regulates a connected network of genes to ensure robust developmental decisions. *PLoS.*
557 *Genet.* 7, e1002179.

558 Hunter,S., Jones,P., Mitchell,A., Apweiler,R., Attwood,T.K., Bateman,A., Bernard,T., Binns,D., Bork,P.,
559 Burge,S., de,C.E., Coggill,P., Corbett,M., Das,U., Daugherty,L., Duquenne,L., Finn,R.D., Fraser,M.,
560 Gough,J., Haft,D., Hulo,N., Kahn,D., Kelly,E., Letunic,I., Lonsdale,D., Lopez,R., Madera,M., Maslen,J.,
561 McAnulla,C., McDowall,J., McMenamin,C., Mi,H., Mutowo-Muellenet,P., Mulder,N., Natale,D., Orengo,C.,
562 Pesseat,S., Punta,M., Quinn,A.F., Rivoire,C., Sangrador-Vegas,A., Selengut,J.D., Sigrist,C.J.,
563 Scheremetjew,M., Tate,J., Thimmajananathan,M., Thomas,P.D., Wu,C.H., Yeats,C., and Yong,S.Y. (2012).
564 InterPro in 2011: new developments in the family and domain prediction database. *Nucleic Acids Res.* 40,
565 D306-D312.

566 Jan,C.H., Friedman,R.C., Ruby,J.G., and Bartel,D.P. (2011). Formation, regulation and evolution of
567 *Caenorhabditis elegans* 3'UTRs. *Nature* 469, 97-101.

568 Joshi,P.M., Riddle,M.R., Djabrayan,N.J., and Rothman,J.H. (2010). *Caenorhabditis elegans* as a model for
569 stem cell biology. *Dev. Dyn.* 239, 1539-1554.

570 Karp,X., Hammell,M., Ow,M.C., and Ambros,V. (2011). Effect of life history on microRNA expression during *C.*
571 *elegans* development. *RNA.* 17, 639-651.

572 Kawahara,H., Okada,Y., Imai,T., Iwanami,A., Mischel,P.S., and Okano,H. (2011). Musashi1 cooperates in
573 abnormal cell lineage protein 28 (Lin28)-mediated let-7 family microRNA biogenesis in early neural
574 differentiation. *J. Biol. Chem.* 286, 16121-16130.

575 Kitano,H. (2004). Biological robustness. *Nat. Rev. Genet.* 5, 826-837.

576 Kudlow,B.A., Zhang,L., and Han,M. (2012). Systematic analysis of tissue-restricted miRISCs reveals a broad
577 role for microRNAs in suppressing basal activity of the *C. elegans* pathogen response. *Mol. Cell* 46, 530-
578 541.

579 Larkin,M.A., Blackshields,G., Brown,N.P., Chenna,R., McGettigan,P.A., McWilliam,H., Valentin,F.,
580 Wallace,I.M., Wilm,A., Lopez,R., Thompson,J.D., Gibson,T.J., and Higgins,D.G. (2007). Clustal W and
581 Clustal X version 2.0. *Bioinformatics.* 23, 2947-2948.

582 Ledwich,D., Wu,Y.C., Driscoll,M., and Xue,D. (2000). Analysis of programmed cell death in the nematode
583 *Caenorhabditis elegans*. *Methods Enzymol.* 322, 76-88.

584 Lehner,B., Tischler,J., and Fraser,A.G. (2006). RNAi screens in *Caenorhabditis elegans* in a 96-well liquid
585 format and their application to the systematic identification of genetic interactions. *Nat. Protoc.* 1, 1617-
586 1620.

587 Lewis,B.P., Burge,C.B., and Bartel,D.P. (2005). Conserved seed pairing, often flanked by adenosines,
588 indicates that thousands of human genes are microRNA targets. *Cell* 120, 15-20.

589 Miska,E.A., varez-Saavedra,E., Abbott,A.L., Lau,N.C., Hellman,A.B., McGonagle,S.M., Bartel,D.P.,
590 Ambros,V.R., and Horvitz,H.R. (2007). Most *Caenorhabditis elegans* microRNAs are individually not
591 essential for development or viability. *PLoS. Genet.* 3, e215.

592 Morita,K. and Han,M. (2006). Multiple mechanisms are involved in regulating the expression of the
593 developmental timing regulator lin-28 in *Caenorhabditis elegans*. *EMBO J.* 25, 5794-5804.

594 Moss,E.G., Lee,R.C., and Ambros,V. (1997). The cold shock domain protein LIN-28 controls developmental
595 timing in *C. elegans* and is regulated by the lin-4 RNA. *Cell* 88, 637-646.

- Moss, E.G. and Tang, L. (2003). Conservation of the heterochronic regulator Lin-28, its developmental expression and microRNA complementary sites. *Dev. Biol.* 258, 432-442.
- Nakagawa, A., Shi, Y., Kage-Nakadai, E., Mitani, S., and Xue, D. (2010). Caspase-dependent conversion of Dicer ribonuclease into a death-promoting deoxyribonuclease. *Science* 328, 327-334.
- Olsson-Carter, K. and Slack, F.J. (2010). A developmental timing switch promotes axon outgrowth independent of known guidance receptors. *PLoS. Genet.* 6.
- Parry, D.H., Xu, J., and Ruvkun, G. (2007). A whole-genome RNAi Screen for *C. elegans* miRNA pathway genes. *Curr. Biol.* 17, 2013-2022.
- Pasquinelli, A.E. and Ruvkun, G. (2002). Control of developmental timing by microRNAs and their targets. *Annu. Rev. Cell Dev. Biol.* 18, 495-513.
- Peden, E., Killian, D.J., and Xue, D. (2008). Cell death specification in *C. elegans*. *Cell Cycle* 7, 2479-2484.
- Pinan-Lucarre, B., Gabel, C.V., Reina, C.P., Hulme, S.E., Shevkoplyas, S.S., Slone, R.D., Xue, J., Qiao, Y., Weisberg, S., Roodhouse, K., Sun, L., Whitesides, G.M., Samuel, A., and Driscoll, M. (2012). The core apoptotic executioner proteins CED-3 and CED-4 promote initiation of neuronal regeneration in *Caenorhabditis elegans*. *PLoS. Biol.* 10, e1001331.
- Punta, M., Coghill, P.C., Eberhardt, R.Y., Mistry, J., Tate, J., Boursnell, C., Pang, N., Forslund, K., Ceric, G., Clements, J., Heger, A., Holm, L., Sonnhammer, E.L., Eddy, S.R., Bateman, A., and Finn, R.D. (2012). The Pfam protein families database. *Nucleic Acids Res.* 40, D290-D301.
- Reddien, P.W., Andersen, E.C., Huang, M.C., and Horvitz, H.R. (2007). DPL-1 DP, LIN-35 Rb and EFL-1 E2F act with the MCD-1 zinc-finger protein to promote programmed cell death in *Caenorhabditis elegans*. *Genetics* 175, 1719-1733.
- Resnick, T.D., McCulloch, K.A., and Rougvie, A.E. (2010). miRNAs give worms the time of their lives: small RNAs and temporal control in *Caenorhabditis elegans*. *Dev. Dyn.* 239, 1477-1489.
- Rickers, A., Brockstedt, E., Mapara, M.Y., Otto, A., Dorken, B., and Bommert, K. (1998). Inhibition of CPP32 blocks surface IgM-mediated apoptosis and D4-GDI cleavage in human BL60 Burkitt lymphoma cells. *Eur. J. Immunol.* 28, 296-304.
- Rougvie, A.E. and Moss, E.G. (2013). Developmental Transitions in *C. elegans* Larval Stages. *Curr. Top. Dev. Biol.* 105, 153-180.
- Rual, J.F., Ceron, J., Koreth, J., Hao, T., Nicot, A.S., Hirozane-Kishikawa, T., Vandenhaute, J., Orkin, S.H., Hill, D.E., van den, H.S., and Vidal, M. (2004). Toward improving *Caenorhabditis elegans* phenome mapping with an ORFeome-based RNAi library. *Genome Res.* 14, 2162-2168.
- Ruvkun, G. and Giusto, J. (1989). The *Caenorhabditis elegans* heterochronic gene *lin-14* encodes a nuclear protein that forms a temporal developmental switch. *Nature* 338, 313-319.
- Sakakibara, S., Imai, T., Hamaguchi, K., Okabe, M., Aruga, J., Nakajima, K., Yasutomi, D., Nagata, T., Kurihara, Y., Uesugi, S., Miyata, T., Ogawa, M., Mikoshiba, K., and Okano, H. (1996). Mouse-Musashi-1, a neural RNA-binding protein highly enriched in the mammalian CNS stem cell. *Dev. Biol.* 176, 230-242.
- Seggerson, K., Tang, L., and Moss, E.G. (2002). Two genetic circuits repress the *Caenorhabditis elegans* heterochronic gene *lin-28* after translation initiation. *Dev. Biol.* 243, 215-225.
- Shaham, S. and Horvitz, H.R. (1996). Developing *Caenorhabditis elegans* neurons may contain both cell-death protective and killer activities. *Genes Dev.* 10, 578-591.
- Slack, F. and Ruvkun, G. (1997). Temporal pattern formation by heterochronic genes. *Annu. Rev. Genet.* 31, 611-634.
- Sriram, S.M., Kim, B.Y., and Kwon, Y.T. (2011). The N-end rule pathway: emerging functions and molecular principles of substrate recognition. *Nat. Rev. Mol. Cell Biol.* 12, 735-747.
- Sulston, J.E. and Horvitz, H.R. (1977). Post-embryonic cell lineages of the nematode, *Caenorhabditis elegans*. *Dev. Biol.* 56, 110-156.
- Suzuki, Y. and Han, M. (2006). Genetic redundancy masks diverse functions of the tumor suppressor gene PTEN during *C. elegans* development. *Genes Dev.* 20, 423-428.
- Taylor, R.C., Brumatti, G., Ito, S., Hengartner, M.O., Derry, W.B., and Martin, S.J. (2007). Establishing a blueprint for CED-3-dependent killing through identification of multiple substrates for this protease. *J. Biol. Chem.* 282, 15011-15021.
- Thacker, C., Sheps, J.A., and Rose, A.M. (2006). *Caenorhabditis elegans* *dpy-5* is a cuticle procollagen processed by a proprotein convertase. *Cell Mol. Life Sci.* 63, 1193-1204.

Than, M.T., Kudlow, B.A., and Han, M. (2013). Functional analysis of neuronal microRNAs in *Caenorhabditis elegans* dauer formation by combinational genetics and Neuronal miRISC immunoprecipitation. *PLoS. Genet.* 9, e1003592.

Timmons, L., Court DL, and Fire, A. (2001). Ingestion of bacterially expressed dsRNAs can produce specific and potent genetic interference in *Caenorhabditis elegans*. *Gene* 263, 103-112.

Ustianenko, D., Hrossova, D., Potesil, D., Chalupnikova, K., Hrazdilova, K., Pachernik, J., Cetkovska, K., Uldrijan, S., Zdrahal, Z., and Vanacova, S. (2013). Mammalian DIS3L2 exoribonuclease targets the uridylated precursors of let-7 miRNAs. *RNA*.

varez-Saavedra, E. and Horvitz, H.R. (2010). Many families of *C. elegans* microRNAs are not essential for development or viability. *Curr. Biol.* 20, 367-373.

Viswanathan, S.R. and Daley, G.Q. (2010). Lin28: A microRNA regulator with a macro role. *Cell* 140, 445-449.

Wu, Y.C., Stanfield, G.M., and Horvitz, H.R. (2000). NUC-1, a *Caenorhabditis elegans* DNase II homolog, functions in an intermediate step of DNA degradation during apoptosis. *Genes Dev.* 14, 536-548.

Xue, D., Shaham, S., and Horvitz, H.R. (1996). The *Caenorhabditis elegans* cell-death protein CED-3 is a cysteine protease with substrate specificities similar to those of the human CPP32 protease. *Genes Dev.* 10, 1073-1083.

Yee, C., Yang, W., and Hekimi, S. (2014). The intrinsic apoptosis pathway mediates the pro-longevity response to mitochondrial ROS in *C. elegans*. *Cell* 157, 897-909.

Yuan, J., Shaham, S., Ledoux, S., Ellis, H.M., and Horvitz, H.R. (1993). The *C. elegans* cell death gene *ced-3* encodes a protein similar to mammalian interleukin-1 beta-converting enzyme. *Cell* 75, 641-652.

Yuan, J.Y. and Horvitz, H.R. (1990). The *Caenorhabditis elegans* genes *ced-3* and *ced-4* act cell autonomously to cause programmed cell death. *Dev. Biol.* 138, 33-41.

Zhang, L., Ding, L., Cheung, T.H., Dong, M.Q., Chen, J., Sewell, A.K., Liu, X., Yates, J.R., III, and Han, M. (2007). Systematic identification of *C. elegans* miRISC proteins, miRNAs, and mRNA targets by their interactions with GW182 proteins AIN-1 and AIN-2. *Mol. Cell* 28, 598-613.

Zhang, L., Hammell, M., Kudlow, B.A., Ambros, V., and Han, M. (2009). Systematic analysis of dynamic miRNA-target interactions during *C. elegans* development. *Development* 136, 3043-3055.

Zhang, X., Zabinsky, R., Teng, Y., Cui, M., and Han, M. (2011). microRNAs play critical roles in the survival and recovery of *Caenorhabditis elegans* from starvation-induced L1 diapause. *Proc. Natl. Acad. Sci. U. S. A* 108, 17997-18002.

Figure titles and legends

Figure 1. Genome-wide RNAi screen for genes that cooperate with miRISCs to regulate development.

(A) Rationale of enhancer screen strategy (detailed in Figure 1—figure supplement 1A). (B) The number of genes identified as interactors of either/both *ain-1(lf)* and/or *ain-2(lf)* (C) Distribution of the 126 interactors into functional categories (interactors listed in supplemental Table 2). (D) The proportion of genes exhibiting singular versus pleiotropic RNAi phenotypes with *ain-1(lf)* or *ain-2(lf)* (detailed phenotypic frequencies shown in Figure 1—figure supplement 1B).

The following figure supplements are available for Figure1:

Figure Supplement 1. RNAi screen strategy and frequencies of phenotypes.

Figure 2. *C. elegans* strains compromised in both miRISC and *ced-3* functions have significant pleiotropic developmental phenotypes. (A and B) Microscopic images showing the pleiotropic phenotypes

of the *ced-3(lf);ain-1(lf)* double mutant, including egg-laying defect (Egl), sluggish movement (Slu), body morphology defects (Bmd), larval arrest (Lva) and embryonic lethality (Emb). Asterisk in (A) indicates an Egl animal that was devoured by internally hatched progeny, and the arrow indicates an adult animal with multiple defects (Egl, Slu and Bmd). Figure 2—figure supplement 1 shows the phenotype of another interactor, *ceh-18*, which is very different from *ced-3*, supporting distinct physiological relevance of the identified interactors. (C) *ced-3(RNAi)* significantly enhanced the frequency of *ain-1(lf)* phenotypes. Mean values \pm SD for percent normal ($p < 0.001$, *compared to wt with mock RNAi, **compared to all others, Chi-square test comparing the distributions of phenotypes). Number of worms tested indicated above each bar (same for all figures). (D) Mean values \pm SD of embryonic lethality ($p < 0.05$ **compared to all, Mann-Whitney test). (E) Enhancement of miRISC phenotypes by *ced-3(lf)* and *ced-4(lf)*. Mean values \pm SD for percent normal ($p < 0.0001$, *compared to each of the relevant single mutants, Chi-square test comparing the distributions of phenotypes). Other *ain-1* and *ced-3* alleles (Figure 2—figure supplement 2) and the *ain-1* interaction with *egl-1* (Figure 2—figure supplement 3) were also tested. (F) Rescue effects of expressing *ain-1* or *ain-2* in specific tissues (driven by tissue-specific promoters for the four principal tissues of *C. elegans* including the hypodermis, gut, muscle, and nerve; see Methods) in the *ced-3(lf);ain-1(lf)* double mutants. “All tissues” indicates a genomic *ain-1* transgene. Mean values \pm SD for percent normal [$p < 0.0001$, Fisher’s Exact test comparing the distribution of normal and abnormal animals for each rescue to *ced-3(lf);ain-1(lf)* without rescue (see Methods for statistical rationale)].

The following figure supplements are available for Figure 2:

Figure Supplement 1. *ain-1(lf);ceh-18(lf)* double mutants have reduced oocytes.

Figure Supplement 2. Additional phenotypes of *ced-3(lf);ain-1(lf)* and test of other alleles.

Figure Supplement 3. The core apoptotic regulatory pathway acts in parallel to miRISC for normal development.

Figure 3. *ain-1(lf)* does not alter cell-death phenotypes. (A) Cartoon illustrating a previously established enhancer assay using a reduction-of-function (*rf*) *ced-3* allele (Reddien et al., 2007). (B) *ain-1(lf)* does not enhance the cell death defect of a *ced-3(rf)* mutation ($p < 0.0001$, *compared to *ced-3(rf)*, Mann-Whitney test). (C) No enhanced interaction between *ain-1(lf)* and *nuc-1(lf)*. Mean values \pm SD (no significant difference, Fisher’s Exact test comparing the distributions of normal and abnormal animals of the *ain-1(lf);nuc-1(lf)* double mutant to the single mutants). (D) *ain-1(RNAi)* does not alter apoptotic events as indicated by L1 head corpses that fail to occur in *ced-3(lf)* mutants. The *ced-1(lf)* mutation was used to enhance visualization of head corpses (Ledwich et al., 2000). Mean values \pm SD (no significant difference, Mann-Whitney test).

Figure 4. Loss of *ced-3* function slows the rate of post-embryonic development. (A) Percent of animals reaching adulthood at 96 hours after hatching is shown. Mean \pm SD ($p < 0.0001$, *compared to wt, **compared

to the relevant single mutants, Fisher's Exact test comparing the distributions of adult to larval-stage animals at this time). (B and C) Distribution of stages at 48 hours and 72 hours with food ($p < 0.0001$, *compared to wt, **compared to the relevant single mutants, Chi-square test comparing the distributions of all stages). Also see Figure 4—figure supplement 1.

The following figure supplements are available for Figure 4:

Figure Supplement 1. *ced-3(lf)* mutants displayed a mild but significant reduction in the rate of post-embryonic development.

Figure 5. Identification of specific miRNAs that cooperate with *ced-3* caspase to regulate development.

(A) Diagram for screening miRNA deletion mutants (listed in supplemental Table 4) when fed mock or *ced-3* RNAi to identify overt developmental phenotypes when *ced-3* was depleted. *let-7(lf)* and *lin-4(lf)* mutants were excluded due to significant defects alone. (B) miRNA deletion(s) [indicated by the miR number(s)] identified in (A) were combined with *ced-3(lf)*. "+" and "-" indicate wild-type and *ced-3(null)*, respectively. Phenotypes including egg-laying defect (Egl), ruptured vulva (Rup), and sluggish movement (Slu) were quantified. Mean values \pm SD for percent normal ($p < 0.05$, *when compared to *ced-3(lf)* and the relevant miRNA deletion(s) alone, Fisher's Exact test comparing the distributions of normal and abnormal animals). (C and D) *ced-3(lf)* enhances adult-specific alae defects including low quality (thin and rough) and gapped alae [bracket in (C) near the mid-body shows a gap]. Percent of adults with alae defects ($p < 0.001$, *compared to the relevant single or double mutants, Chi-square test comparing the distributions of adult alae phenotypes).

Figure 6. *ced-3* may act upstream of multiple conserved pluripotent factors to affect differentiation of stem cell-like seam cells.

(A and B) Pseudocolored GFP from DIC images of a seam cell reporter and dot plot quantitation. The tick line depicts 16 seam cells that are normally found in wild-type animals. Black bars indicate the median values for each strain ($p < 0.0001$, *compared to wt, **compared to single mutants, Mann-Whitney test). (C) Effect of RNAi treatment beginning at L2 on the seam-cell-number phenotype of the *ced-3(lf);ain-1(lf)* double mutant ($p < 0.0001$, *compared to mock RNAi, Mann-Whitney test). *C. elegans disl-2* is homologous to mammalian Dis3l2 (Figure 6—figure supplement 1). (D) Effect of the same RNAi on the the *ced-3(lf);ain-1(lf)* double mutant defects. Mean values \pm SD for percent normal [$p < 0.0001$, *compared to mock RNAi, Fisher's Exact test comparing the distributions of normal and abnormal animals (see Methods for statistical rationale)].

The following figure supplements are available for Figure 6:

Figure Supplement 1. Protein sequence alignment of human DIS3L2 and *C. elegans* DISL-2.

Figure Supplement 2. Additional analyses of seam cells for the *ced-3(lf);ain-1(lf)* double mutant.

Figure Supplement 3. *ced-3(lf)* mutants enhance *lin-66(RNAi)* ruptured vulva phenotype.

Figure 7. CED-3 cleavage of LIN-14, LIN-28, and DISL-2 (DIS3L2) *in vitro*. (A) Established *in vitro* CED-3 cleavage assay (Xue et al., 1996) of ³⁵S-labeled proteins. CED-9 served as a positive control throughout. Red asterisks indicate cleavage products (same in B-D). (B) Result from a longer-run gel showing near quantitative cleavage of full-length DISL-2 (arrow indicates the full-length protein). (C) *In vitro* cleavage assay with the zDEVD-fmk caspase-specific irreversible inhibitor (Rickers et al., 1998). The arrow and arrowhead (and red asterisks) indicate the full-length protein and a predominant CED-3 cleavage product, respectively. (D) Effect of the D31A mutation on CED-3 cleavage (for other mutants see Figure 7—figure supplement 1). (E) Diagram showing the position and consequence of LIN-28A cleavage by CED-3 *in vitro* (22kDa with an N-terminal asparagine). Each panel was performed as an independent experiment.

The following figure supplements are available for Figure 7:

Figure Supplement 1. Mutagenesis of LIN-28A to identify the CED-3 cleavage site.

Figure Supplement 2. Identification of possible CED-3 cleavage sites in LIN-14 and DISL-2.

Figure 8. *In vivo* confirmation that CED-3 caspase negatively regulates LIN-28 expression in late larval stages.

(A) Western blot with the LIN-28 antibody we developed (validation shown in Figure 8—figure supplement 1) to see the effects of *ced-3(lf)* mutations on LIN-28 protein expression during developmental transitions. Notice that the cleavage product of the larger isoform of LIN-28 observed in the *in vitro* assay (Figure 7) is not detectable in the *in vivo* analysis, suggesting that the cleavage product, which has an Asn instead of Met as the N-terminal end residue, may potentially be sensitive to the N-end rule proteasomal degradation pathway. The pattern and timing of LIN-28 expression and downregulation we show here for wt are similar to previous findings (Morita and Han, 2006; Seggerson et al., 2002) and two independent *ced-3(lf)* mutant strains are shown here (quantitation is shown in Figure 8—figure supplement 1C). (B-C) Pseudocolored GFP from DIC images of L3 larvae near the mid-body. Also see DIC images of these animals without GFP illumination (Figure supplement 2A) and test of similar staging (Figure supplement 2B). Size bars are indicated. “wt” indicates the *lin-28(+):gfp* integrated transgene alone previously shown to be functional (Moss et al., 1997) and “*ced-3(lf)*” indicates this same transgene combined with a *ced-3(lf)* mutation. (D) Quantitation of the LIN-28::GFP expression between the strains within the L3 stage. ($p=0.0038$, significant compared to wt, Mann-Whitney test comparing the integrated intensity of LIN-28::GFP hypodermal expression in L3 larvae). Persistent expression of LIN-28::GFP in head cells (Figure 8—figure supplement 2D,E)

The following figure supplements are available for Figure 8:

Figure Supplement 1. Validation of our newly generated LIN-28 antibody and Western blot quantitation.

Figure Supplement 2. Larval staging and persistent LIN-28::GFP expression.

Figure 9. CED-3 caspase represses LIN-28 *in vivo* to ensure proper temporal cell fate patterning regulation. (A) Effects of disrupting CED-3 activity on LIN-28 *in vivo* on the rate of post-embryonic growth. Percent of animals reaching adulthood at 96 hours after hatching is shown. “+” indicates the *lin-28(+):gfp* integrated transgene described in Figure 8B-C. D31A indicates a transgene integration with the CED-3-cleavage-resistant D31A point mutation in the first exon of LIN-28 but is otherwise identical to the original (+) transgene. Test of *lin-28(lf)* rescue (Figure 9—figure supplement 1) and copy number of the transgenes (Figure 9—figure supplement 2). Mean values \pm SD ($p < 0.0001$, *compared to wt(+), Fisher’s Exact test comparing the distributions of adult to larval-stage animals at this time). (B-C) Western blot for the LIN-28::GFP transgenes described in (A) and quantitation from three independent Western blot experiments of the LIN-28::GFP transgenes [one Western blot shown in (B)]. Here, 1.0 was defined as the intensity of total LIN-28(D31A)::GFP at 0hr normalized to actin. Both the *lin-28(+)* and the *ced-3(lf);lin-28(+)* strains and the 30hr time point for all strains were compared to this value. Mean \pm SEM for the two time points (dashed lines are used only to indicate the net change in relative expression for the three strains). (D) Disrupting CED-3 activity on LIN-28 enhances adult alae defects of the strains described in (A) ($p < 0.01$, *compared to wt(+), Chi-square test comparing the distributions of adult alae phenotypes). Figure 9—figure supplement 3 shows examples of the adult alae phenotypes for these three strains. Data for increased expression of LIN-14 in *ced-3(lf)* mutants at the first larval stage is shown in Figure 9—figure supplement 4.

The following figure supplements are available for Figure 9:

Figure Supplement 1. Test for *lin-28(D31A)* function in overcoming the *lin-28(n719,lf)* protruding vulva defect.

Figure Supplement 2. Transgene copy number determination.

Figure supplement 3. Loss of *ced-3* function or mutating the CED-3 cleavage site of LIN-28 enhances adult alae defects by a multi-copy *lin-28* transgene.

Figure Supplement 4. LIN-14 protein levels are increased in *ced-3(lf)* mutants at the first larval stage.

Figure 10. Model for CED-3 function in temporal cell fate patterning regulation. (A) Model of CED-3 collaborating with miRNAs to repress the expression of LIN-14, LIN-28, and DISL-2. Red blocks indicate the new findings. For simplicity, many other factors in the pathway were not included here including additional regulators associated with this pathway that were also identified in our genomic enhancer screen (see Figure 10—figure supplement 1). (B) Hypothetical model for the biochemical role of CED-3 cleavage in protein turnover during development whereby a new N-terminus is generated which could potentially destabilize the protein according to the N-end rule (see text).

The following figure supplements are available for Figure 10:

Figure Supplement 1. A more detailed genetic model for roles of CED-3 caspase in regulating the heterochronic pathway and for showing other genes from our genomic screen in this pathway.

Supplemental Materials:

Figure Supplements with Legends

Supplemental Tables

Statistics Source Data

Titles and legends of supplemental figures, tables and source data:

Figure 1—figure supplement 1. RNAi screen strategy and frequencies of phenotypes. (A) Cartoon diagram illustrating steps of the screen performed for the entire ORF RNAi library using liquid culture 96 well format. We included the RNAi-sensitizing mutation, *rrf-3(lf)*, with *ain-1(lf)* and *ain-2(lf)* to increase screen sensitivity and therefore used *rrf-3(lf)* alone for the control. In the double blind, we identified genes where the RNAi effect for the control was mostly normal but where *ain-1(lf)* or *ain-2(lf)* showed an obvious enhancer phenotype (as defined in supplemental Table 1). Example phenotypes body morphology defect (Bmd), embryonic lethality (Emb), and reduced brood size (Red) are depicted for illustration purposes only. Confirmations were performed in quadruplicate in the double blind. These interactors were all then revealed and sequence-verified. (B) Frequency of phenotypes observed in the RNAi screen. The three letter phenotypes indicated here are all defined in supplemental Table 1 and are depicted here as the frequency of occurrence amongst interactors for either *ain-1* or *ain-2*. Due to pleiotropism, the sum of the phenotypes will exceed 100 percent. All genes identified in the screen with individual phenotypes are listed in supplemental Table 2.

Figure 2—figure supplement 1. *ain-1(lf);ceh-18(lf)* double mutants have reduced oocytes. DIC images of gonads from single and double mutant animals. (A) Arrows indicate the farthest point for the gonad turn. Asterisks are located near the first identifiable oocyte in the given gonad arm. The expanded segment is a digital zoom in to show the morphological detail of the double mutant gonad for the indicated segment. (B) Dot plot of the oocyte counts per gonad arm ($n = 40$ for each strain). Each dot represents the number of oocytes in one gonad arm and the median values are given by black bars for each strain ($p < 0.001$, *compared to *ain-1(lf)* and **compared to both *ain-1(lf)* and *ceh-18(lf)* alone, Mann-Whitney test).

The distinct phenotypes observed amongst some of the genetic interactors, such as *ced-3* (shown in Figure 2) versus *ceh-18* suggest distinct physiological functions and argue against general sickness of the single mutants. This conclusion is also supported more broadly by the frequency of phenotypes observed (Figure 1—figure supplement 2) such that equal frequency is not observed across the various phenotypes.

Figure 2—figure supplement 2. Additional phenotypes of *ced-3(lf);ain-1(lf)* and test of other alleles. (A) *ain-1(lf)* animals treated with *ced-3(RNAi)* have a significant increase in oocytes laid ($p < 0.0001$, *compared to

wt mock, **compared to all others, Mann-Whitney test). **(B)** Developmental defects associated with *ced-3(lf);ain-1(lf)* double mutants were observed for other *ain-1(lf)* and *ced-3(lf)* alleles. Bar graph showing the synergistic effect between *ain-1(tm3681)* and two *ced-3(lf)* alleles on the egg-laying defective (Egl) phenotype. Animals were scored 5 days after eggs were placed on plates. The mean values are shown (** $p < 0.001$ compared to wt and each of the relevant single mutants, Fisher's exact test). **(C)** Phenotypes of adults scored at two time points after synchronized first stage larvae were placed on OP50 food. In panel C, and elsewhere in the study, unless noted, the *ain-1(ku322)* and *ced-3(n1286)* alleles were used (** $p < 0.001$, relative to wt and single mutants, Fisher's exact test comparing the distribution of normal and abnormal animals). **(D)** The *ced-3(lf);ain-2(lf)* double mutant adults are phenotypically comparable to the *ced-3(lf)* single mutant adults in **(C)** at 96 hours on OP50 food following synchronization ($p < 0.001$, Chi-square analysis). For all panels: Slu, sluggish or immobile; Egl, egg-laying defective; Rup, ruptured through vulva. Number of worms tested is indicated above each bar.

Figure 2—figure supplement 3. The core apoptotic regulatory pathway acts in parallel to miRISC for normal development. **(A)** Core apoptotic regulatory pathway with *C. elegans* gene names indicated (mammalian counterparts in parentheses). **(B)** The phenotypes observed for *ced-3(lf);ain-1(lf)* were observed when combining *ain-1(lf)* with RNAi of upstream components of the *ced-3* pathway. The *ain-1(lf)* single mutant shows enhanced defects when treated with *ced-3*, *ced-4*, or *egl-1* RNAi for two RNAi generations. Significance of phenotypes when wt and *ain-1(lf)* animals were fed the indicated RNAi was determined [$**p < 0.001$, relative to both *ain-1(lf)* fed mock RNAi and to wt fed the given RNAi, Fisher's exact test comparing the distributions of normal and abnormal animals (see Methods for statistical rationale)].

Figure 4—figure supplement 1. *ced-3(lf)* mutants displayed a mild but significant reduction in the rate of post-embryonic development. **(A and B)** Animals were synchronized 36 h in M9 buffer at 20°C then placed on standard bacteria food (OP50) and staged every 24 hours thereafter. Data for 24 and 96 hours are shown here and data for 48 and 72 hours are shown in Figure 4B-C. The distribution of animals from first larval stage (L1) through young adult/adult (indicated as YA+) is shown ($p < 0.0001$, *compared to wt, Chi-square analysis comparing the distributions of stages). Number of worms indicated above each set.

Figure 6—figure supplement 1. Protein sequence alignment of human DIS3L2 and *C. elegans* DISL-2. Domain prediction and sequence alignment of the mammalian DIS3L2 protein with the *C. elegans* DISL-2 protein. Domain predication was done by Interpro (Hunter et al., 2012) and Pfam (Punta et al., 2012), and the alignment was done using Clustal W (Larkin et al., 2007).

Figure 6—figure supplement 2. Additional analyses of seam cells for the *ced-3(lf);ain-1(lf)* double mutant. **(A)** Diagram depicting the symmetric and asymmetric cell divisions of V1-V4 and V6 lineages [based

on content detailed in a recent review (Rougvie and Moss, 2013)]. One cell is shown beginning at L1 (red). In wt, the L2 stage has a symmetric division followed by asymmetric divisions thereafter. The *lin-28(lf)* mutation generates a precocious phenotype without the L2-specific symmetric division; whereas, the *lin-28(gf)* mutation generates a retarded phenotype with further L2-like reiterations. Thus, a normal animal hatches with 10 seam cells that result in 16 terminally differentiated seam cells by adulthood. (B) The *ced-3(lf);ain-1(lf)* double mutant animals hatch with the correct number of seam cells which continue to develop during late larval stages. Ten seam cells are observed for all strains with no significant differences observed. Black bars indicate the median values for each strain ($p > 0.05$, Mann-Whitney test, all single and double mutants compared to wild-type). (C) Quantitation of third and fourth larval stages of the *ced-3(lf);ain-1(lf)* double mutant animals suggests supernumerary seam cells continue to arise during late larval stages. Black bars indicate the median values for each strain ($p = 0.008$, *compared to L3 stage *ced-3(lf);ain-1(lf)*, Mann-Whitney test). The data shown for the L4 animals in panel B here are unique from the main Figure 6B and are not repeated.

Figure 6—figure supplement 3. *ced-3(lf)* mutants enhance *lin-66(RNAi)* ruptured vulva phenotype. *lin-66* was previously shown to limit the expression of LIN-28 by an incompletely understood mechanism (Morita and Han, 2006). We therefore tested if loss of *ced-3* could enhance the vulva defect in *lin-66(RNAi)*. (A) Images and (B) bar graph showing that *lin-66(RNAi)* increases the frequency of ruptured vulva of both *ced-3(lf)* and *ain-1(lf)* mutants. L2 stage animals were fed either mock or *lin-66(RNAi)* and the subsequent generation was scored for ruptured vulva (Rup) at adulthood (multiple ruptured animals are indicated by arrows). RNAi was used due to the fourth larval stage lethality of the *lin-66(lf)* alleles. *ain-1* in miRISC is already known to negatively regulate LIN-28 expression and its enhancer phenotype here with *lin-66(RNAi)* serves as a positive control. The percent mean values are shown (number of worms indicated above each bar, ** $p < 0.001$, Chi-square analysis).

Figure 7—figure supplement 1. Mutagenesis of LIN-28A to identify the CED-3 cleavage site. Several possible cleavage sites exist in the *C. elegans* LIN-28A protein corresponding to the tetra-peptide D(E,N,G)xxD(E) cleavage sequence with the alternate residues indicated in parentheses and the proximal residue for cleavage underlined (aspartic acid in this position strongly favored) (Xue et al., 1996). (A-B) Mutants were made for the second acidic residue in the tetra-peptide sequence for all such sites in the LIN-28A N-terminal region but only the DVVD to DVVA mutation (noted as D31A in panel B and Figure 7D) abolished CED-3 cleavage. Cleavage products are indicated by red asterisk. These experiments were run independently of those shown in Figure 7 and thus constitute replicates for the mutant D31A cleavage assay.

Figure 7—figure supplement 2. Identification of possible CED-3 cleavage sites in LIN-14 and DSL-2. Numerous possible CED-3 cleavage sites are found in LIN-14B and DSL-2 based on the consensus motif detailed in Figure 7—figure supplement 1 (Xue et al., 1996). (A-B) Potential CED-3 substrate tetrapeptides are

shown in red font, some of which overlap. Closed triangles and open triangles indicate potential cleavage sites of high and moderate probability, respectively. The numbers in parentheses above the sequences indicate the proximal acidic residue. The LIN-14B isoform is shown in (A) since this is the isoform we cloned. However, all of the predicted cleavage sites shown here are also present in the LIN-14A isoform, which differs in the amino terminus prior to the first predicted site.

Figure 8—figure supplement 1. Validation of our newly generated LIN-28 antibody and quantitation of Western blot data. (A) Western blot to demonstrate the specificity of our peptide-purified rabbit-anti-*C. elegans* LIN-28 antibody. The peptide we chose to immunize the rabbits with is found near the C-terminus (reported in Methods) and therefore should recognize both the a and b isoforms equally well. Equivalent amounts of extracts from mixed staged wt, *lin-28(n719,lf)*, and a strain with an integrated transgene of *lin-28::GFP* were resolved by SDS-PAGE then probed with our purified LIN-28 antibody. The *Is[lin-28::gfp]* strain shows both the endogenous forms of LIN-28 and the shifted fusion protein. (B) The large isoform of LIN-28 (corresponding to the a isoform) was synthesized *in vitro* then added at increasing amounts into the *lin-28(n719,lf)* strain to simulate a complex mixture for all other background proteins. Three exposures of the same gel are shown. Two predominant background bands from the *in vitro* lysate are indicated by dashed blue lines. LIN-28-specific bands (identified in panel A) are indicated. The *lin-28(n719)* + mock lane has as much *in vitro* lysate as the most +LIN-28a lane but with a mock vector to show lysate background. This background is not present in the worm extracts (compare the *lin-28(n719)* lane versus *lin-28(n719)* + mock). (C) Quantitation of Western blot data from Figure 8A. Arbitrarily, 100% was defined as the intensity of total LIN-28 at 0hr normalized to actin for the wt strain. Both *ced-3(lf)* strains were set relative to the wt 0hr. The subsequent time points for all strains were compared to this 0hr value.

Figure 8—figure supplement 2. Larval staging and persistent LIN-28::GFP expression. (A-C) Analysis of gonad length in LIN-28(+) transgenic lines with *ced-3(wt)* or *ced-3(lf)*. We first picked L3 stage animals in the blind on a non-fluorescent microscope. Prior to GFP illumination, we assessed the sub-stages of animals by measuring the gonad length of the animals. This was done since the animals had roller phenotype making P cell division difficult to observe and strong defects in LIN-28, directly, are known to have only minor effects on gonad development (Ambros, 1997). Thus, these strains should not be expected to have significant defects in gonad extension and gonad length should serve as a quantifiable metric of larval stage similar to previous reports (Ambros and Horvitz, 1984; Moss et al., 1997; Abbott et al., 2005). The images shown here (A-B) are from the same animals shown in the main Figure 8B-C. The white bars indicate 20 μ M. The white brackets indicate the gonads of equal length. (C) No significant difference in gonad length for the L3 samples was observed between the two strains suggesting similar sub-stage. Mean \pm SD is shown ($p > 0.05$, Mann-Whitney test). (D-E). Pseudocolored GFP from DIC head images of L3 larvae and quantitation of the number of cells expressing LIN-28::GFP ($p < 0.0001$, *compared to wt(+), Chi-square test comparing the distributions of L3

larvae based on the number of LIN-28::GFP positive cells). “+” indicates the *lin-28(+):gfp* integrated transgene previously shown to be functional (Moss et al., 1997). This set of experiments was done completely independently of the ones shown in main Figure 8B-D. A similar method for selection of L3 animals in the blind on a non-fluorescent microscope was used. All animals were visualized for GFP positive cells through multiple focal planes of the head. All images were taken with identical exposure times and all cells were counted by an individual who did not take the images.

Figure 9—figure supplement 1. Test for *lin-28(D31A)* function in overcoming the *lin-28(n719,lf)* protruding vulva defect. The full name of the extrachromosomal array that we tested: *Ex[lin-28(D31A)::gfp::lin-28 3'UTR; myo-3::mCherry; pBSIIKS(-)]* where *myo-3::mCherry* served as the transgenic marker. **(A)** Myo-3::mCherry positive animals are rescued for the Pvl phenotype similar to the original *lin-28(+):gfp* described previously (Moss et al., 1997). The top panel shows two adults not carrying the array which displayed the protruding vulva (Pvl) and ruptured vulva (Rup) (arrows) phenotype, respectively. Three adults carrying the array are indicated in this same panel by an asterisk near their well-developed vulva (also *myo-3::mCherry* positive). The bottom two panels show magnified images of two different animals, one without array, and therefore Pvl, and one with the array, and therefore not Pvl. **(B)** The array-positive animals have a significant rescue compared to animals without the array (89% rescued on average, $p < 0.0001$, *when compared to animals without the array, Fisher's Exact test) showing that the D31A mutation does not alter the gross function of the protein. Rather, we conclude that the D31A mutation only abolishes the direct cleavage of LIN-28 as supported by our *in vitro* experiments (Figure 7 and Figure 7—figure supplement 1). The offspring from parents bearing the rescue array may have some maternal effect with ~10% of adults not carrying the array without Pvl but with severe egg-laying defect (also suggests a non-functional vulva) and the remaining 5% with apparently normal vulva.

Figure 9—figure supplement 2. Transgene copy number determination. + indicates the [*lin-28(+):gfp::lin-28 3'UTR; rol-6*] integrated transgene which was previously published as functional (Moss et al., 1997). **D31A** indicates the transgene integration we generated which contains the D31A point mutation in the first exon of LIN-28. Following integration, total DNA was used as input for qPCR to quantify the copy number. Mean \pm SD is from two sets of *lin-28* primers normalized to two sets of unrelated endogenous genes (*ain-1* and *hrp-1*). These findings suggest low copy number integration for the two transgenes.

Figure 9—figure supplement 3. Loss of *ced-3* function or mutating the CED-3 cleavage site of LIN-28 enhances adult alae defects by a multi-copy *lin-28* transgene. **(A-D)** Adult alae were scored using DIC optics (quantitation of findings is shown in Figure 9D). These images serve only as visual reference for the phenotypes scored. The strains are described in Figure 9—figure supplements 1-2.

Figure 9—figure supplement 4. LIN-14 protein levels are increased in *ced-3(lf)* mutants at the first larval stage. An integrated transgenic strain *Is[lin-14::gfp]* previously published (Olsson-Carter and Slack, 2010) was crossed with a *ced-3(lf)* mutation. Sibling offspring were isolated to obtain the *Is[lin-14::gfp]* (with wild-type *ced-3* gene) and the *ced-3(lf);Is[lin-14::gfp]*. Results from three independent Western blots of three independent synchronous first stage larvae are shown here. Samples were synchronized, collected, processed, probed by Western blot with an anti-GFP antibody (Clontech, Antibody JL8) independently at different times. Though the difference between wild-type and *ced-3(lf)* is subtle, it is repeatable. The subtle effects seen for LIN-14 are also of note since it is, in part, an upstream positive regulator of *lin-28*. Thus, subtle effects may be physiologically significant.

Figure 10—figure supplement 1. A more detailed genetic model for roles of CED-3 caspase in regulating the heterochronic pathway and for showing other genes from our genomic screen in this pathway. Modified from the discussion provided by a recent review (Rougvie and Moss, 2013), this model is still simplified given the complex and dynamic process (Slack and Ruvkun, 1997; Rougvie and Moss, 2013; Resnick et al., 2010; Pasquinelli and Ruvkun, 2002; Ambros, 1989; Ambros, 2000). Black arrows and blocks indicate aspects of the pathway that were previously known. Red blocks and font indicate the major findings of this study. Blue font indicates factors known to function in this pathway that were also identified in our enhancer screen (supplemental Table 2) as genetic interactors of GW182 (*ain-1* and/or *ain-2*). The blue asterisk associated with *let-7* is to indicate that we also identified the *let-7* family miRNAs in our miRNA-*ced-3* enhancer screen (Figure 5A,B) and that *ced-3(lf)* was able to enhance their specific temporal cell fate patterning phenotypes as seen with adult-specific alae defects (Figure 5D). The blue asterisks and dashed red lines for *miR-1* and *miR-246* indicate additional miRNAs we identified in our miRNA-*ced-3* enhancer screen (Figure 5 A,B). Both *miR-1* and *miR-246* are predicted to target *lin-14* mRNA (see methods) but have not been experimentally demonstrated to do so here. They failed to show enhanced specific developmental timing defects and were not pursued further. Dashed arrows and blocks are intended to indicate a combination of complex direct and indirect effects ultimately affecting developmental fate and timing. ** Previous works have indicated DAF-12 functions on several components of the pathway (Rougvie and Moss, 2013) (Hochbaum et al., 2011), providing the basis for us to have observed the enhanced developmental defects associated with *ain-1(lf)* and *daf-12(RNAi)* (supplemental Table 2). The exact mechanism of LIN-66 function is still unclear (dashed block) though it is able to negatively regulate LIN-28 function (Morita and Han, 2006). MSI-1 (Musashi-1) was identified as an RNA-binding protein that may be important for LIN-28-mediated regulation of pre-miRNA processing as well as translational regulation (Kawahara et al., 2011; Sakakibara et al., 1996). Interestingly, we also identified the *C. elegans* musashi-1 ortholog, *msi-1*, as an enhancer in our screen (supplemental Table 2). Following binding by LIN-28, pre-*let-7* is poly-uridylated by a TUTase (poly-U-polymerase) to mark it for destruction. PUP-2 is indicated here as a *C. elegans* ortholog for TUTase and it was also identified in our screen (supplemental Table 2). Recently, the RNase, Dis3l2 (Dis-3-like RNase gene 2),

was identified as the 3'-5' exonuclease that degrades poly-uridylated-pre-*let-7* miRNA and is the RNase mutated in Perlman syndrome (Ustianenko et al., 2013; Kawahara et al., 2011; Chang et al., 2013). We suggest that the *C. elegans* gene F48E8.6 is the *C. elegans* ortholog of Dis3l2 and have therefore named it DISL-2 (Dis-3-like RNase gene 2) (see Figure 6—figure supplement 1). The intricate network of regulatory factors shown here emphasizes the importance of this pathway and how CED-3 caspase cooperates with the miRISC and numerous other factors to control temporal cell fate patterning.

Supplemental Table 1: Definition of phenotypes scored in this study.

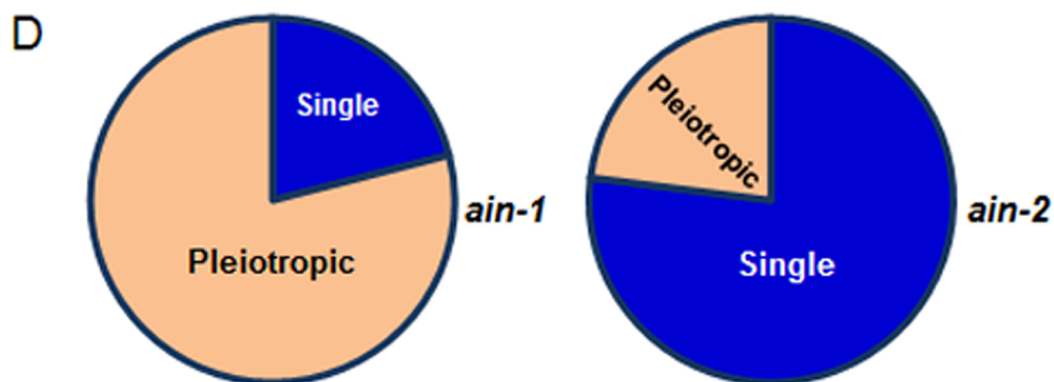
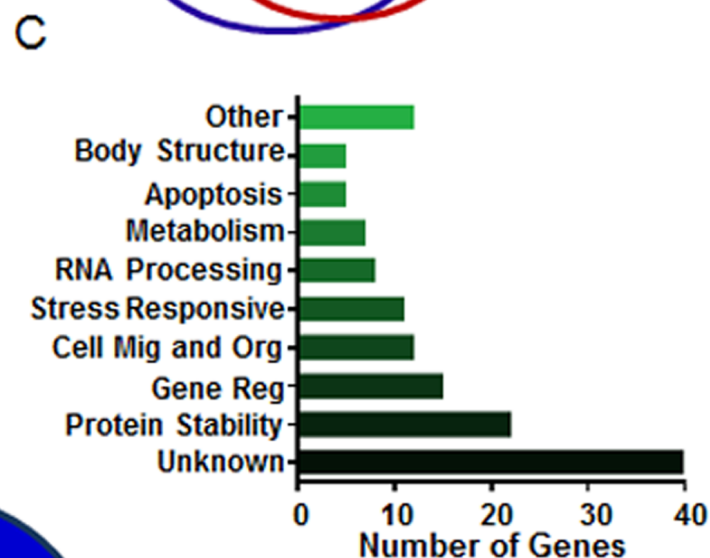
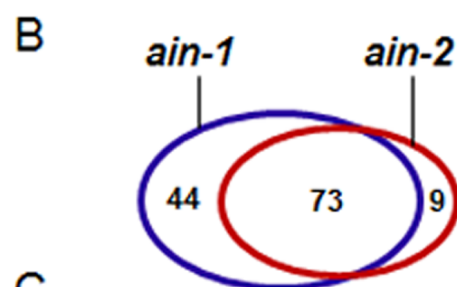
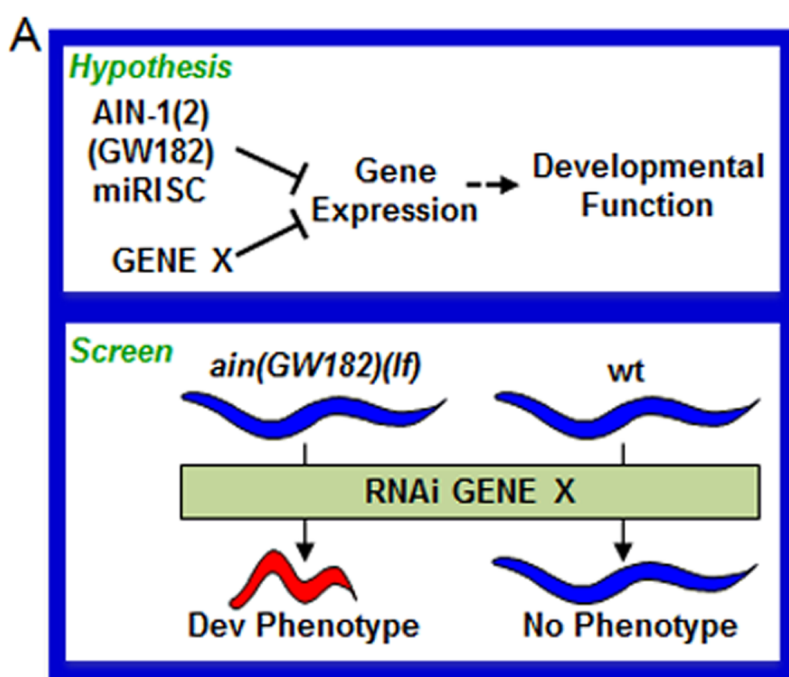
Supplemental Table 2: List of *ain-1* and *ain-2* genetic interactors identified in this study and their relevant phenotypes in brief. RNAi clones are listed alphabetically by gene name. Relevant phenotypes indicated for the given strains are defined in supplemental Table 1.

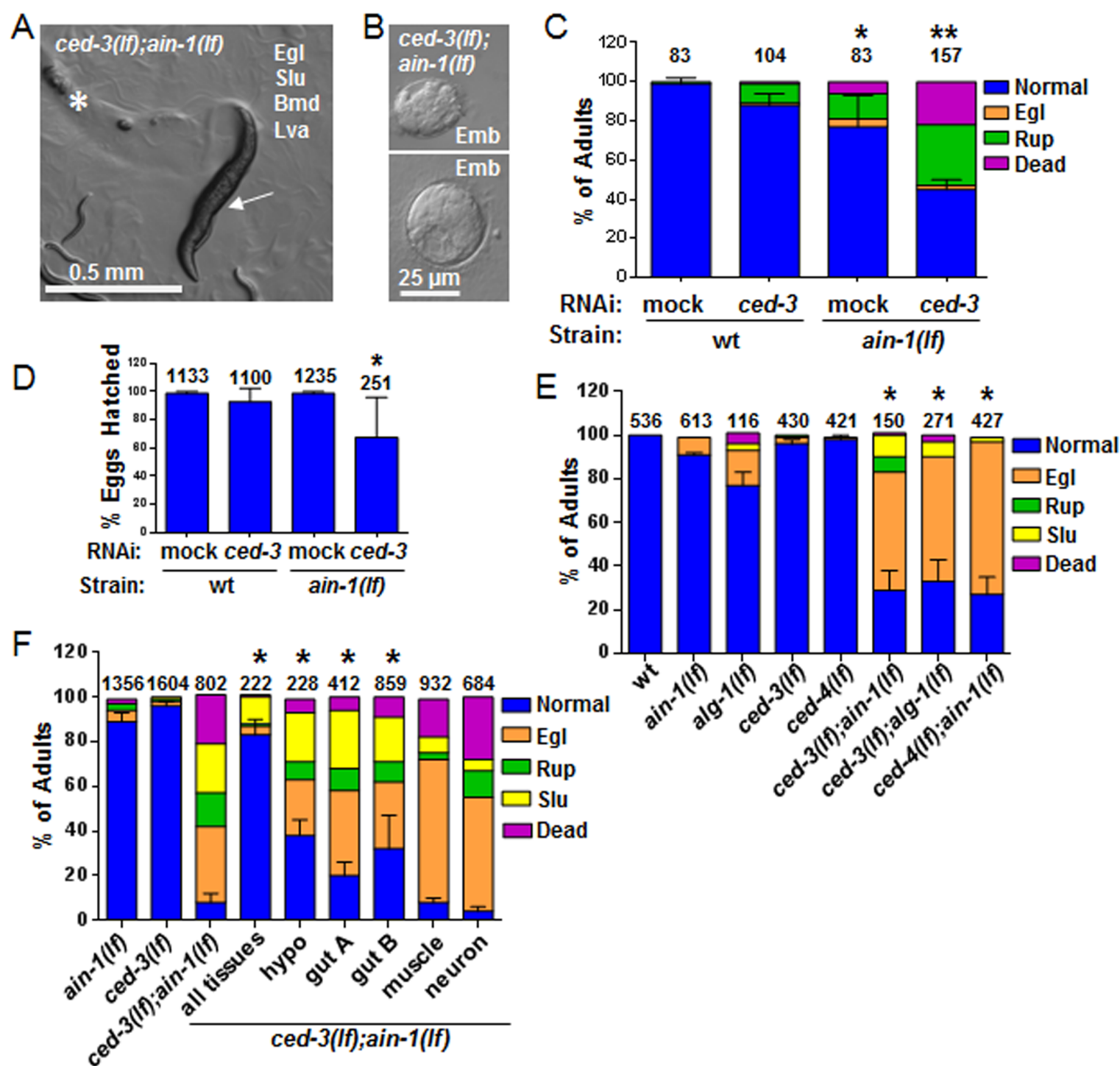
Supplemental Table 3: Phenotypes observed for reverse confirmation test with *ain-1* and *ain-2* RNAi. Effects indicated are relative to the given mutant strain phenotype on mock RNAi. These are results for one generation on the indicated RNAi and not with RNAi enhancing mutations.

Supplemental Table 4: List of *C. elegans* strains and relevant genotypes used in this study.

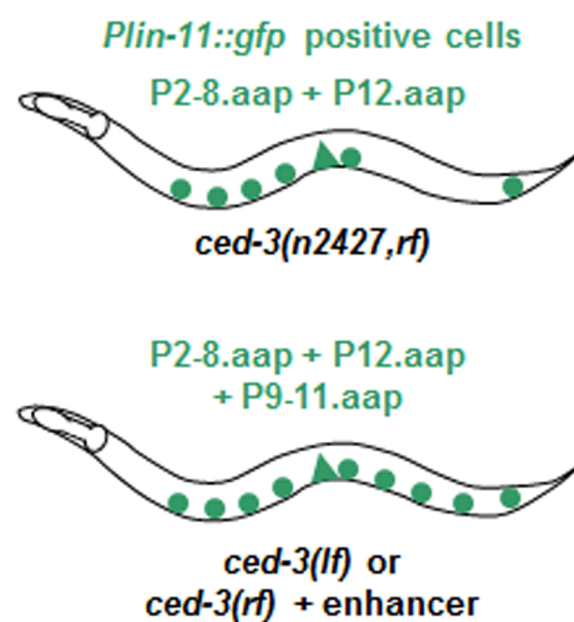
Source data files:

Excel files containing source data for all figures.

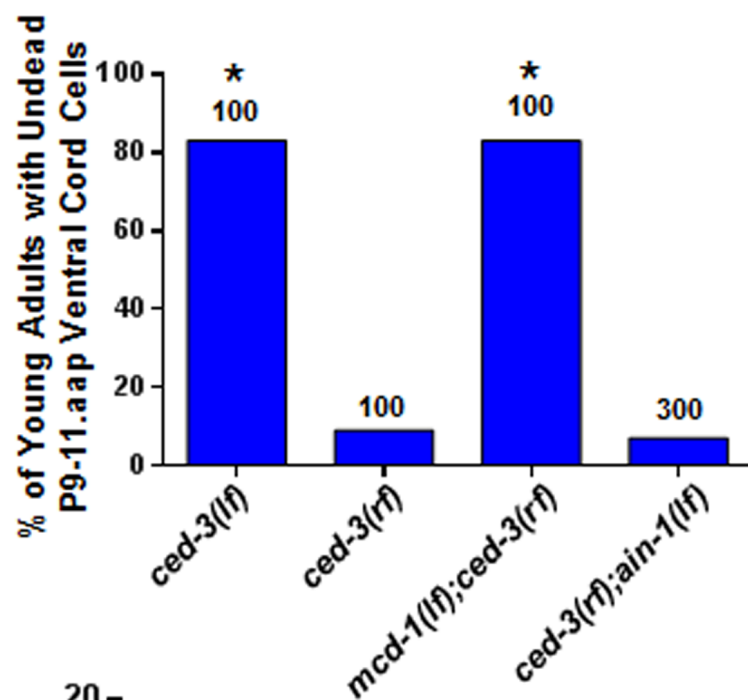




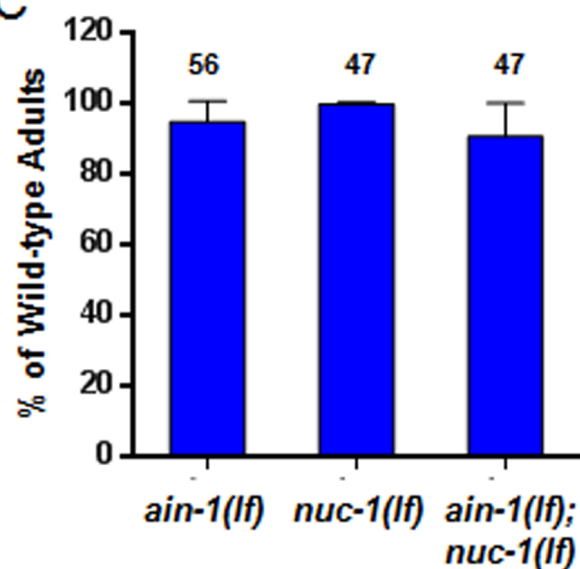
A



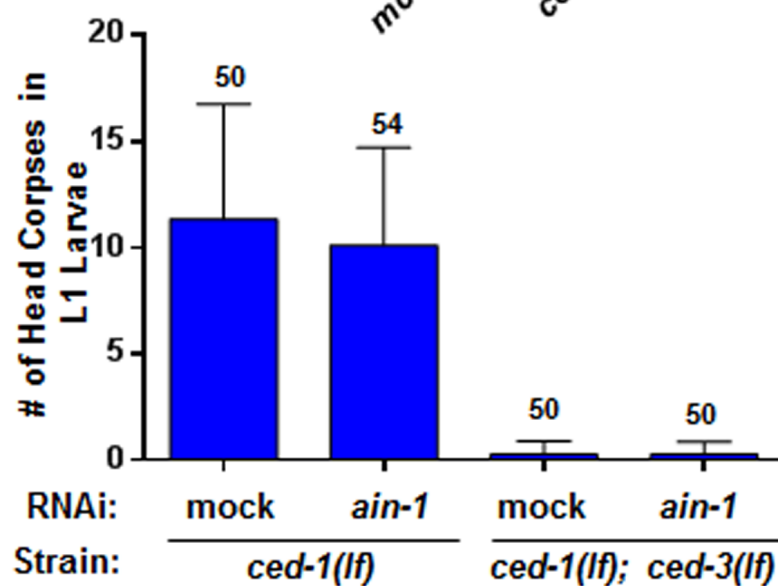
B



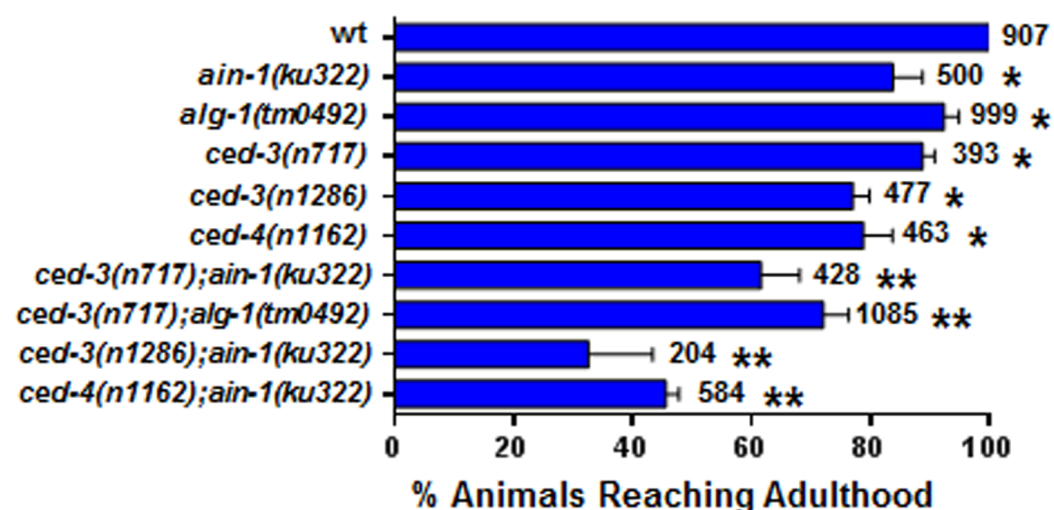
C



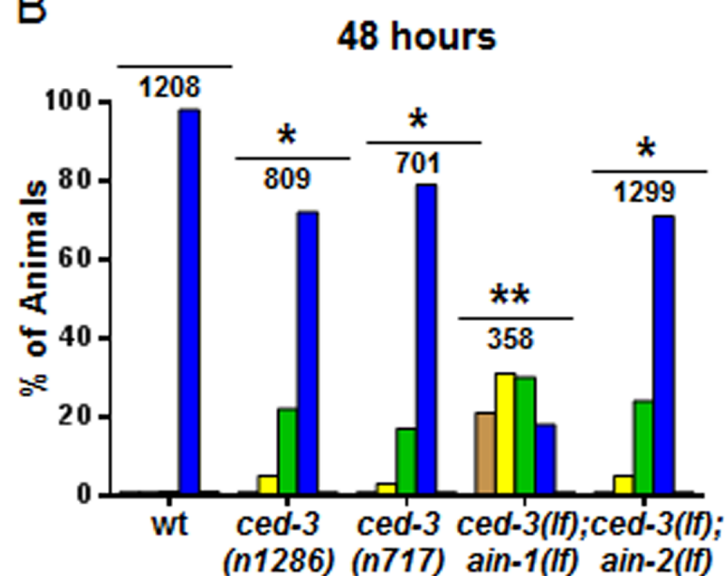
D



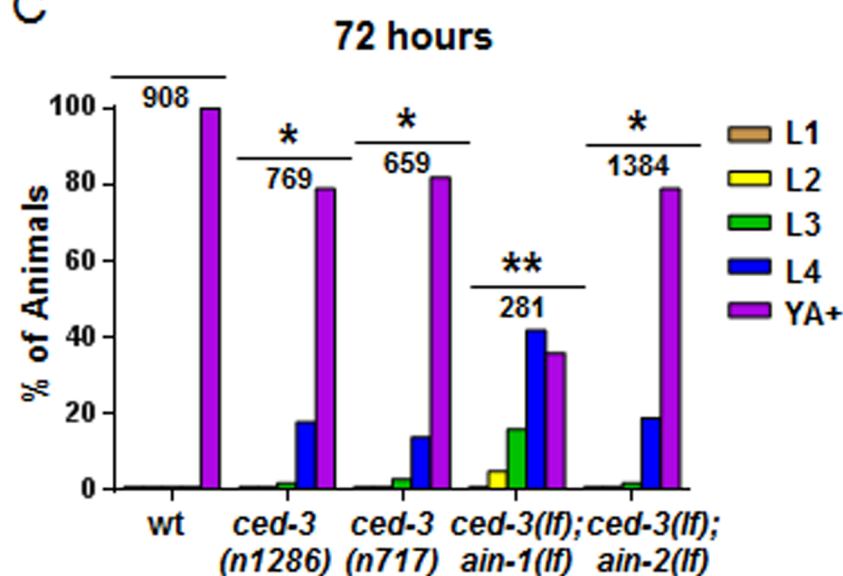
A

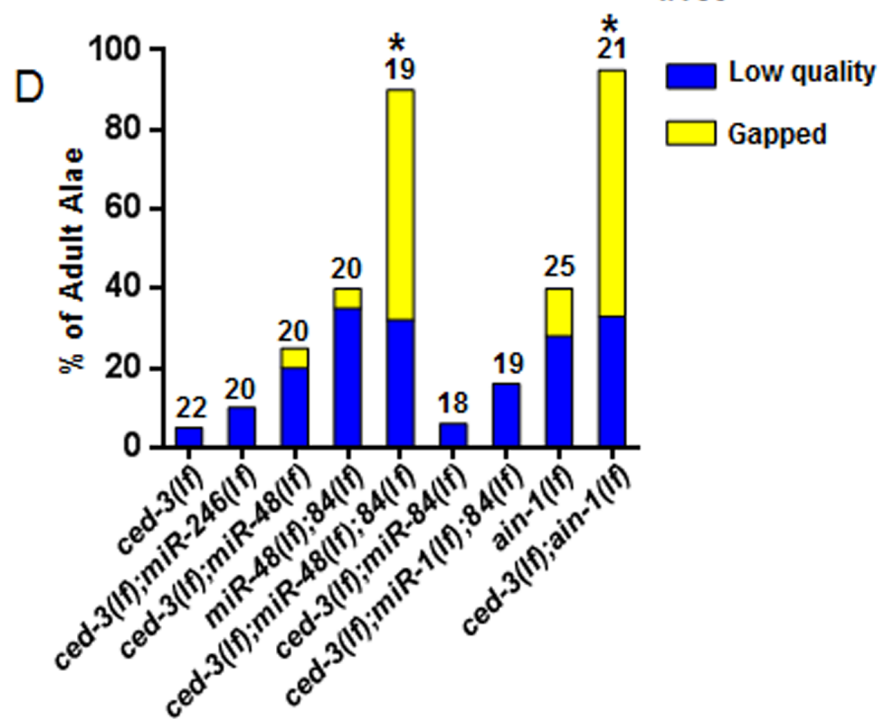
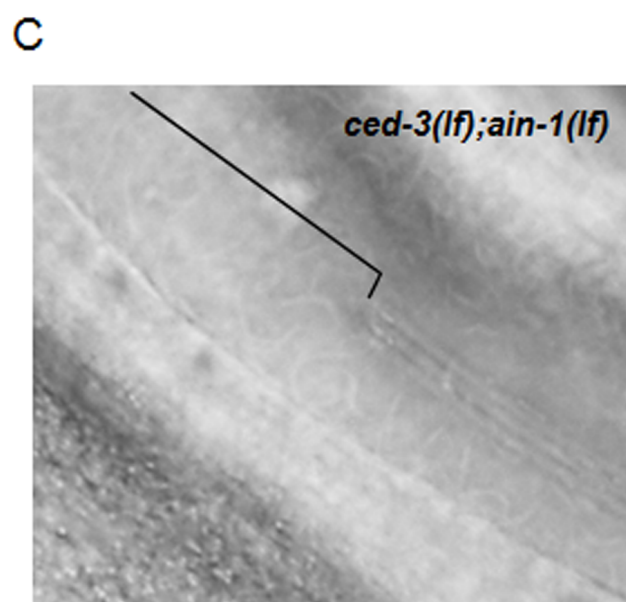
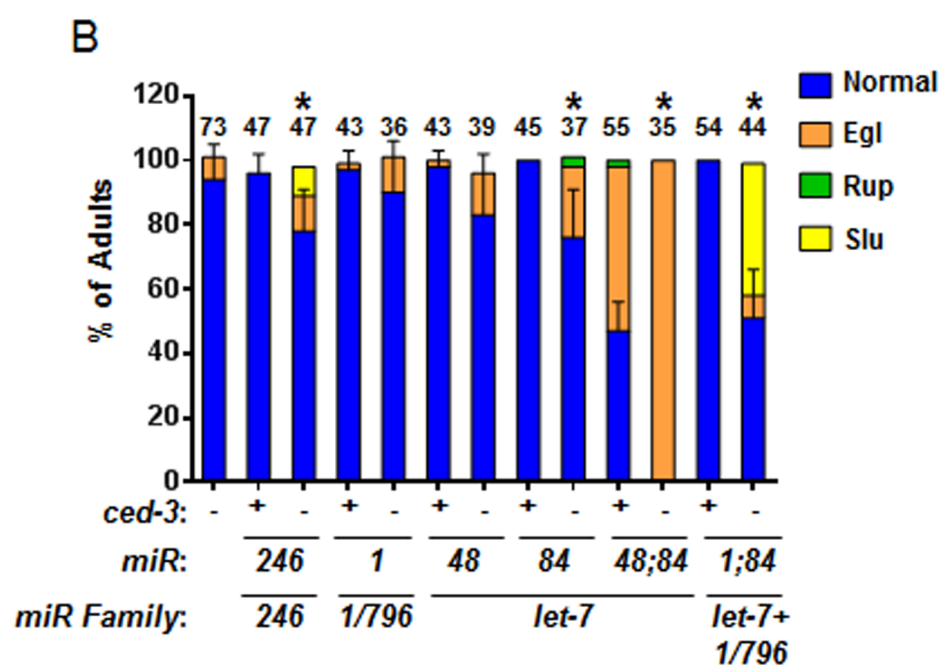
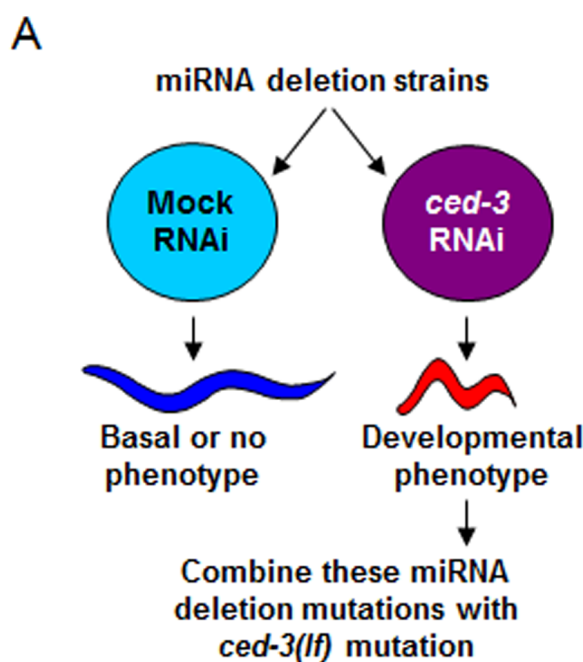


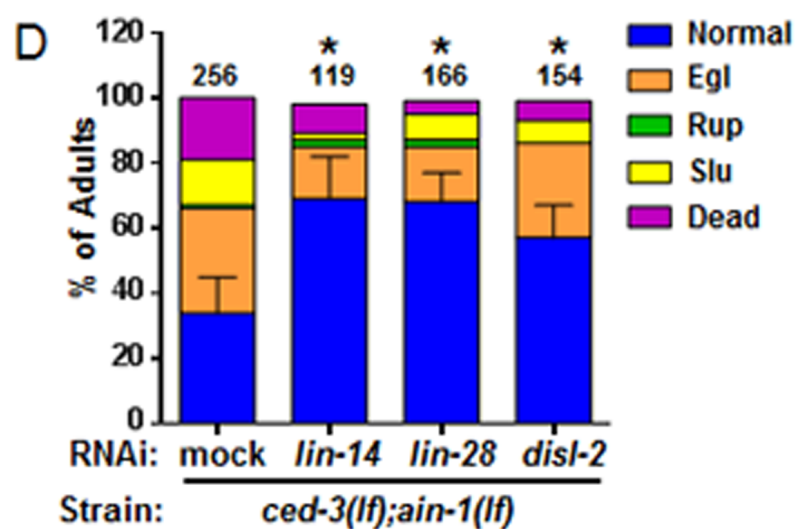
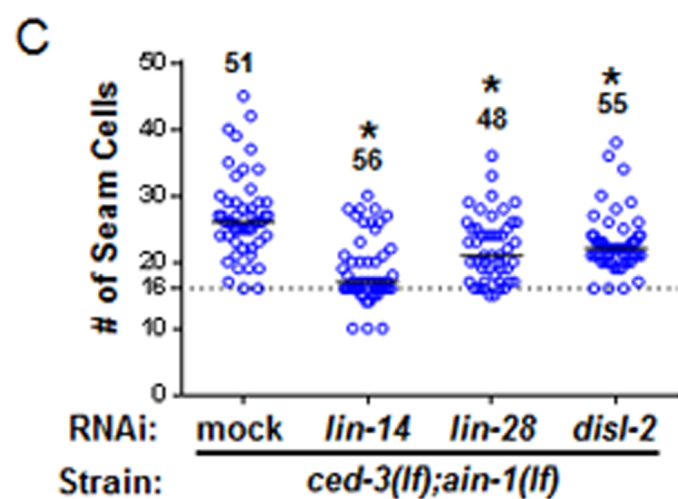
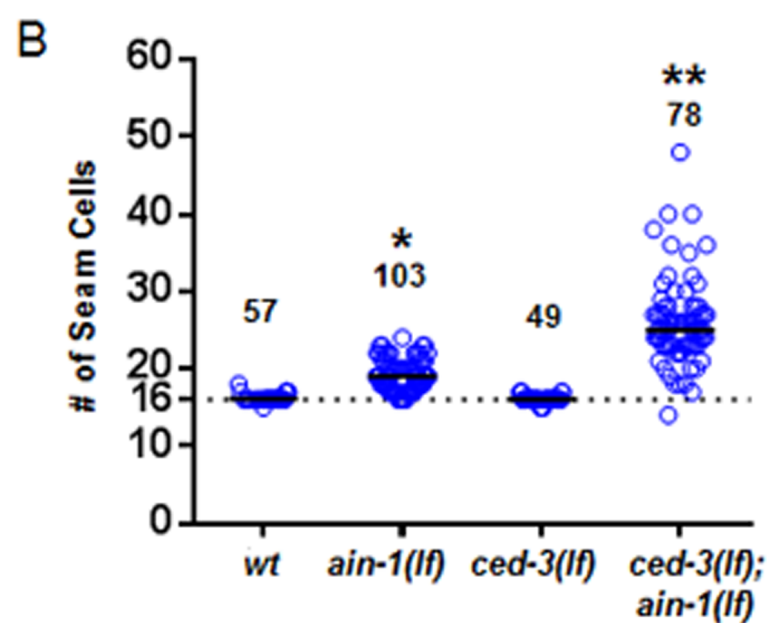
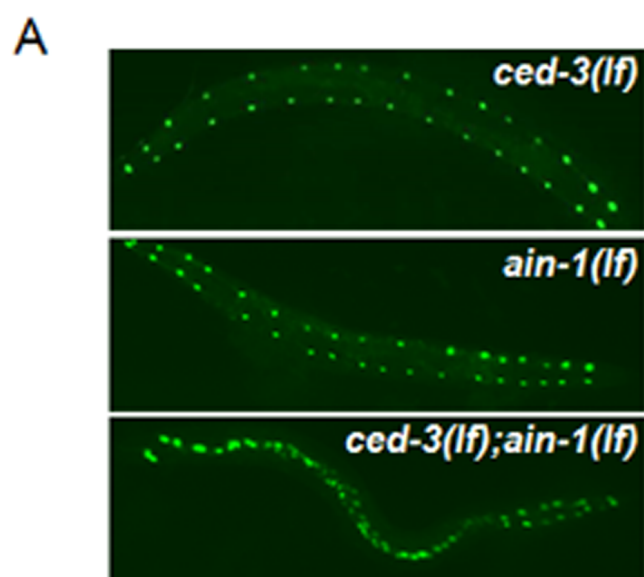
B

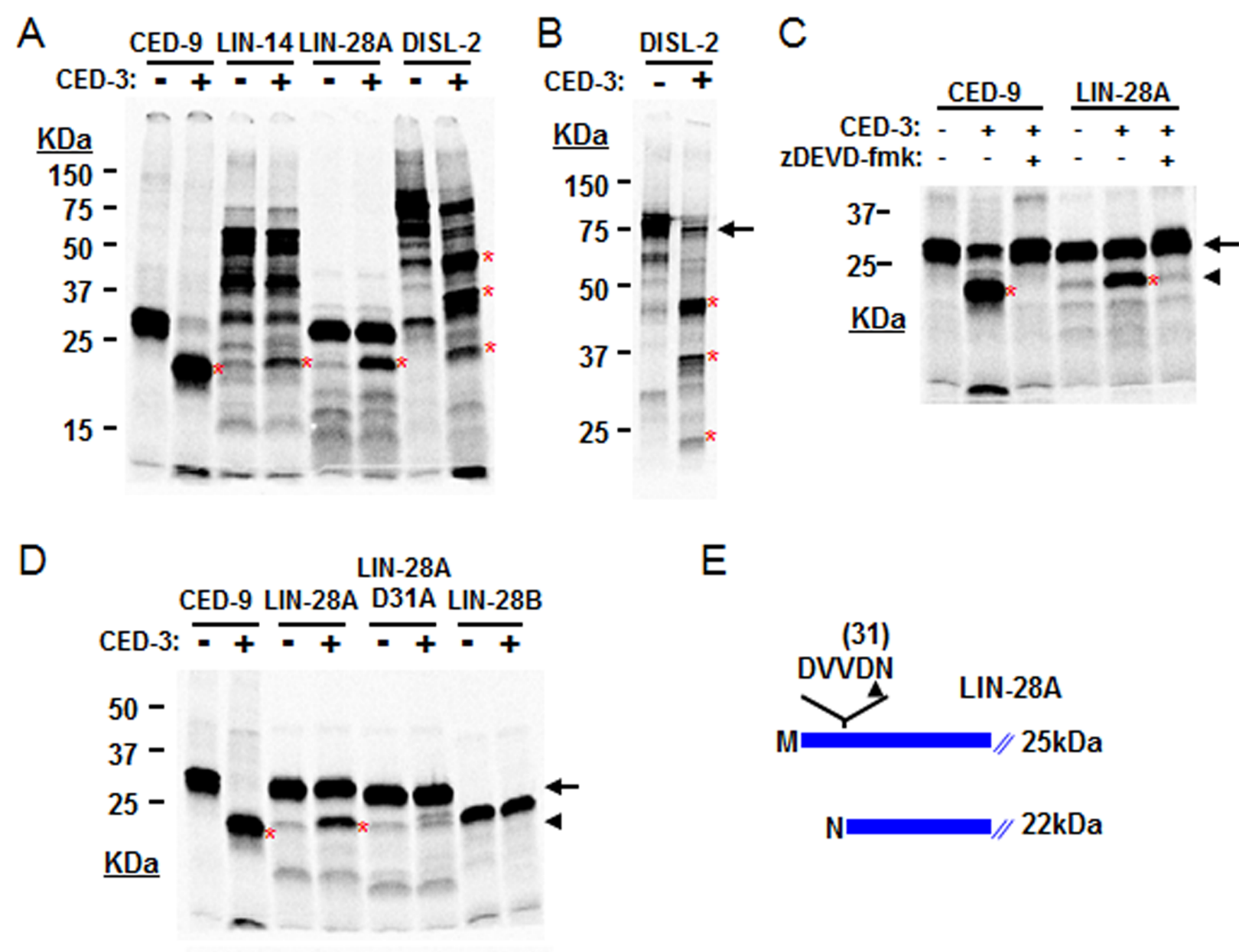


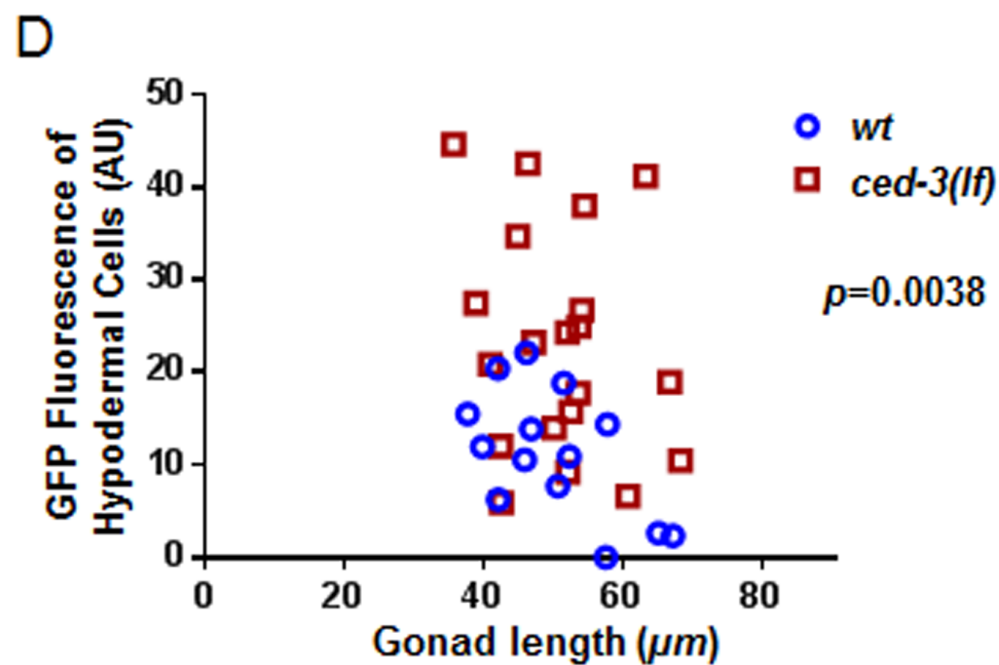
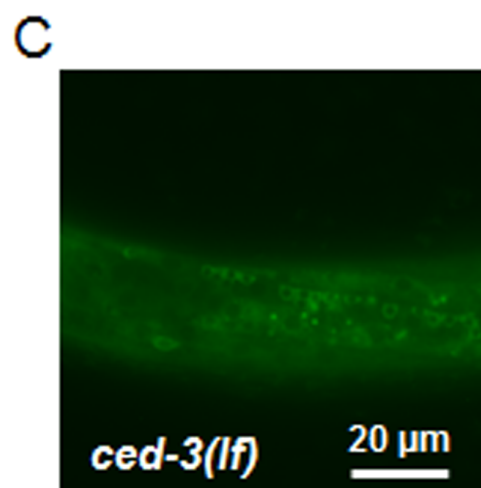
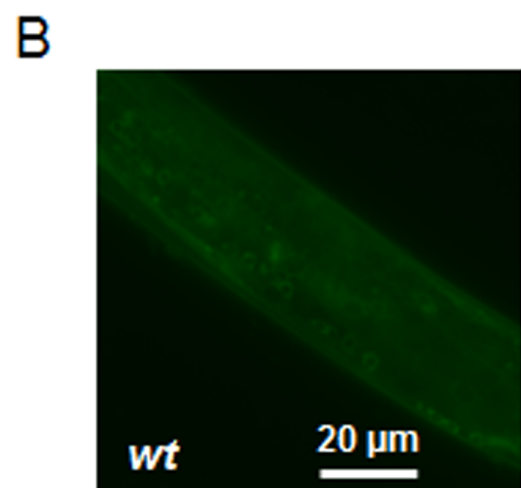
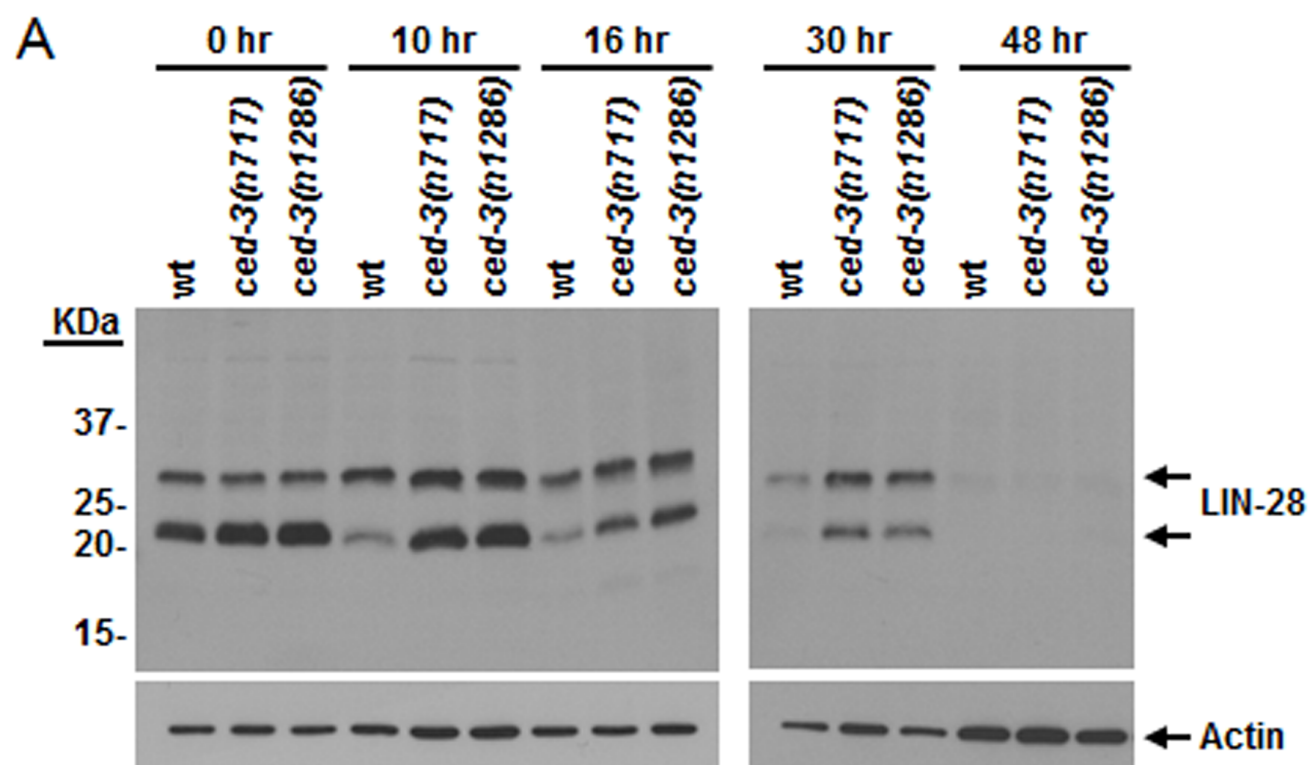
C



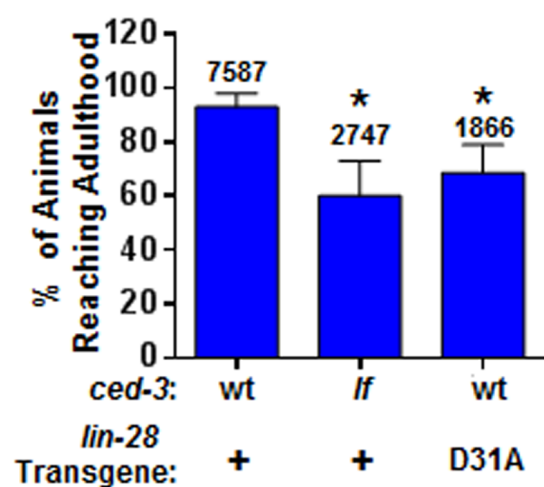




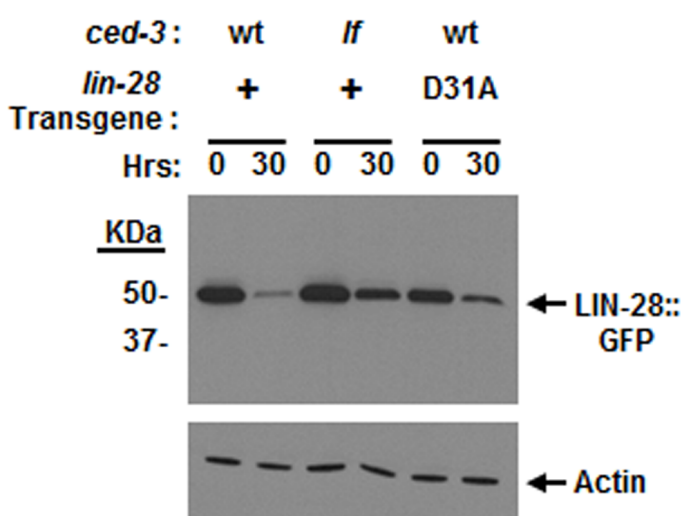




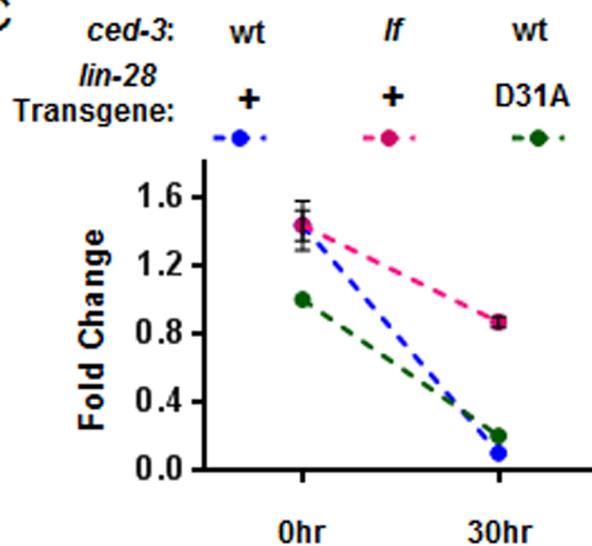
A



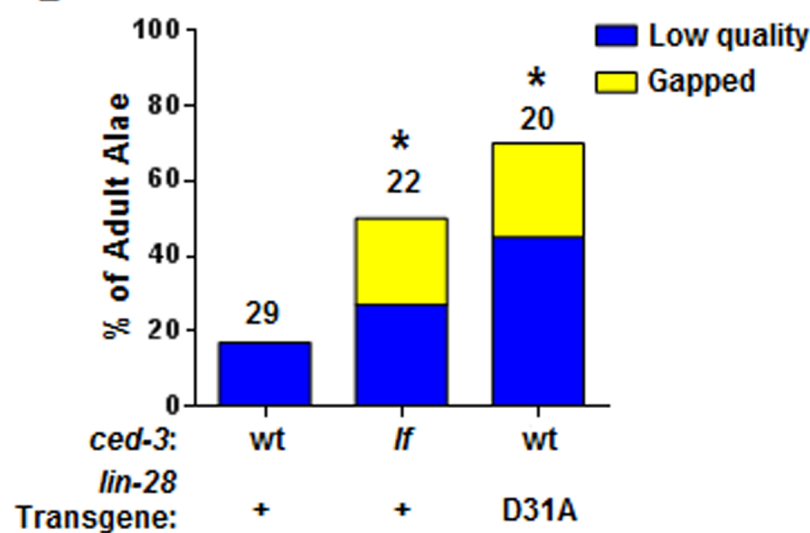
B



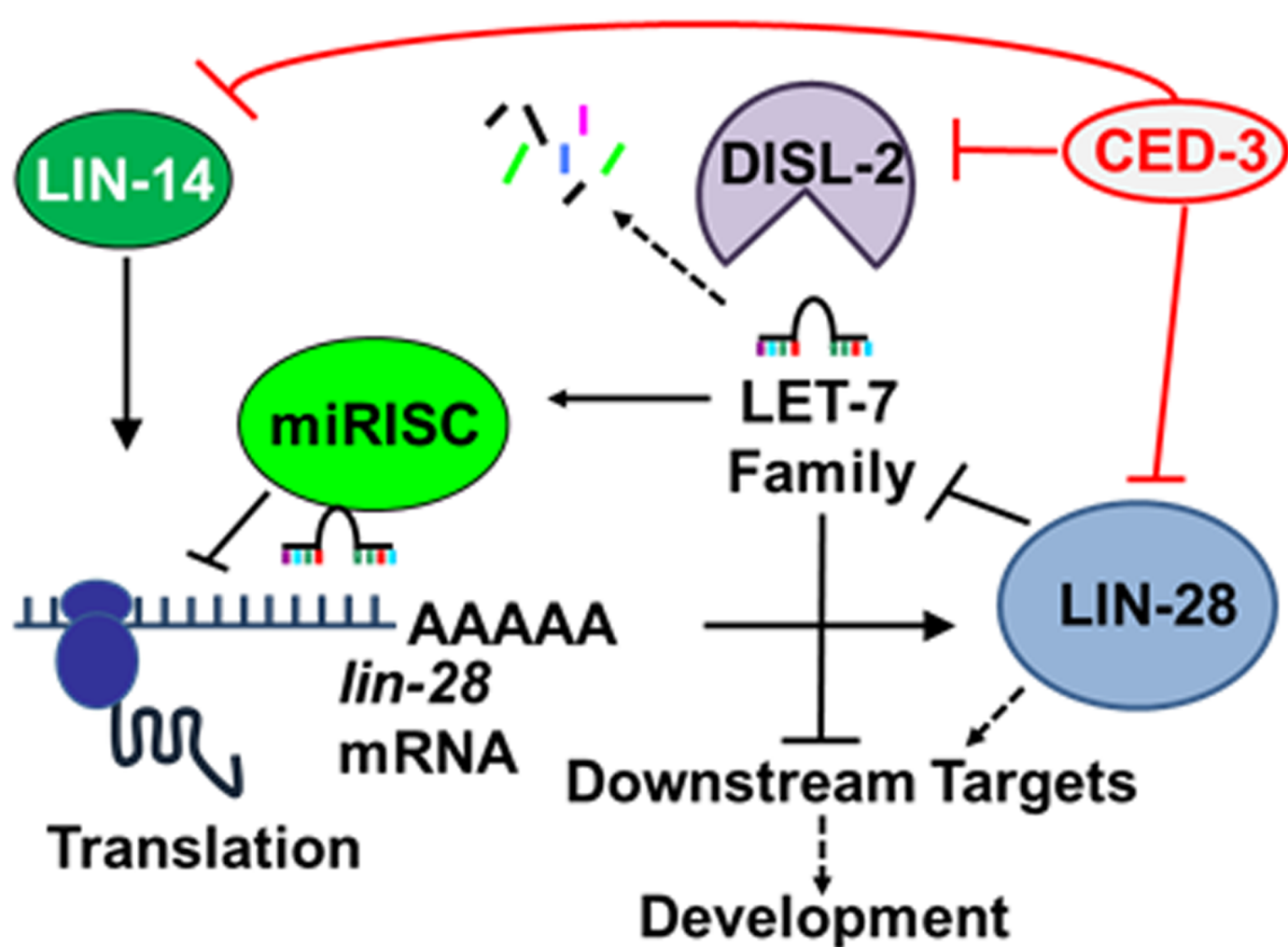
C



D



A



B

